Scientia Iranica B (2018) 25(3), 1215–1235

Sharif University of Technology
Scientia Iranica
Transactions B: Mechanical Engineering
http://scientiairanica.sharif.edu

Unsteady double-diffusive natural convection with Soret and Dufour effects inside a two-sided lid-driven skewed enclosure in the presence of applied magnetic field

O. Ghaffarpasand*

Department of Physics, University of Isfahan, Isfahan 81746, Iran.

Received 26 July 2016; received in revised form 5 January 2017; accepted 8 April 2017

KEYWORDS
Double-diffusive natural convection;
Soret and Dufour effects;
Lewis number;
Buoyancy ratio;
Skewed cavity.

Abstract. This article describes the heat and mass transfer as well as the entropy generation in an unsteady double-diffusive natural convection with Soret and Dufour effects in the presence of an external magnetic field. The analysis uses a two-dimensional skewed enclosure, where the inclined walls make a skew angle λ with x-axis. The governing equations in the physical domain are transformed into an orthogonal computational domain by co-ordinate transformations, and then are solved using a finite-volume method based on SIMPLE algorithm. The computations are carried out in the six skewed enclosures with skew angles $\lambda = 15°, 30°, 45°, 60°, 75°$, and $90°$, for a wide range of the Hartman number, Lewis number, buoyancy ratio, and Dufour coefficient, while Soret coefficient is kept constant at 0.25 in most parts of the study. Results show that the fluid flow, heat and mass transfer, as well as the entropy generation are sensitive to some extent to the skew angle variation. Meanwhile, the Lewis number and buoyancy ratio have aiding and opposing actions, respectively, on suppression effect of Lorentz force against convective heat and mass transfer. It is also shown that the average entropy generation is an increasing function of Lewis number, buoyancy ratio, and Dufour coefficient, while it is a decreasing function of Hartman number.

1. Introduction

Double-diffusive convection problem has received widespread attention in recent years due to its wide applications to various engineering areas such as cooling of electronic systems [1], cooling of nuclear reactors [2], crystal growth in liquids [3], metal manufacturing processing [4], solar power collectors [5], etc. Double-diffusive convection refers to the buoyancy-driven flow induced by combined temperature and concentration gradients [6,7]. Meanwhile, heat and mass transfer has become more complicated than the process of pure thermal natural convection, whereby both science and technology are required to develop advanced models and research methods to facilitate a deeper understanding of the relevant processes involved in this field. As a comprehensive and typical flow problem, the double-diffusive convection is a strong and complex nonlinear coupled process, mainly controlled and influenced by parameters such as buoyancy ratio, Prandtl number, Lewis number, and aspect ratio [8].

Considerable research works have been found in the literature on this problem with different types of enclosures. For instance, Al-Amiri et al. [9] examined numerically the effects of Richardson number, Ri, buoyancy ratio, B, and Lewis number, Le, on double-diffusive mixed convection flow in a lid-driven cavity.

*. *Tel.: +98(0)313-7934843; Fax: +98(0)313-7934800*
E-mail address: o.ghaffarpasand@gmail.com

doi: 10.24200/sci.2017.4497

Results show that the heat and mass transfer can be improved with further decrease of Richardson number. Mahapatra et al. [10] also carried out numerical simulations to study the effects of uniform and non-uniform heating of walls on double-diffusive natural convection in a lid-driven square enclosure. Results indicate that the boundary layer thickness reduces as the buoyancy ratio enhances. Azad et al. [11] studied numerically double-diffusive convection in an open channel with a circular heater on its bottom wall. It has been shown that the heat and mass transfer improve with the rise of Lewis number. Kareem et al. [12] analyzed numerically the unsteady mixed convection heat transfer in a three-dimensional closed cavity with a constant heat flux on the centre part of the bottom wall. They found that increasing the Reynolds number causes an enhancement in the heat transfer across the cavity. Thermo-solutal mixed convection in a rectangular enclosure with sliding top lid was studied by Bettaibi et al. [13] with a new numerical technique. They utilized a numerical method based on the Multiple Relaxation Time (MRT) and Lattice Boltzmann Method (LBM), whereas the temperature and concentration fields were computed by the Finite-Difference Method (FDM). Their results were found to be in acceptable agreement with those of the former published studies. Wang et al. [14] used a regularized LBM model to investigate double-diffusive convection in a vertical enclosure. It has been found that the heat and mass transfer rates decrease with the increase of the aspect ratio.

One of the innovative techniques to control natural convection of electrically conducting fluids is applying an external magnetic field. This technique has numerous applications to engineering areas such as nuclear power plant or nuclear reactor, crystal growth, chemical processes, etc. However, although a significant number of studies are available in the literature on double-diffusive convection, the corresponding researches regarding the role of external magnetic field in control of thermo-solutal combined convection are quite sparse. Kefayati [15] utilized a Finite-Difference Lattice Boltzmann Method (FDLBM) to analyse the effect of magnetic field on double-diffusive mixed convection of shear-thinning fluids in a two-sided lid-driven cavity. Results show that the enhancement of Hartman number causes the decline of heat and mass transfer for multifarious buoyancy ratios and power-law indexes. Mondal and Sibanda [16] studied numerically an unsteady double diffusive convection in an inclined cavity in the presence of a transverse magnetic field. Results indicate that fluid flow and transport phenomena, heat and mass transfer, are significantly dependent on the magnetic field strength and cavity inclination angle. Borhan Uddin et al. [17] studied numerically the effect of buoyancy ratio on unsteady thermo-solutal combined convection in a lid-driven trapezoidal enclosure in the presence of magnetic field. Results show that both heat and mass transfer are developed to some extent by the buoyancy ratio. However, Lewis number and buoyancy ratio are two important parameters which can significantly affect the heat and mass transfer of double-diffusive convection. The investigation of the influence of those parameters on flow pattern and transport phenomena can deepen our understanding of the thermo-solutal combined convection problem.

In the most cited studies of double-diffusive natural convection, important parameters of Soret and Dufour coefficients have been neglected, because they are of smaller order of magnitude compared to the effects described by Fourier and Fick's laws. Nevertheless, when temperature and concentration gradients are large in some applications such as chemical reactors, solidification of binary alloys, groundwater pollutant migration, hydrology and geosciences, the Soret and Dufour effects should be taken into consideration to complete the accurate simulation. The Soret and Dufour effects are called SD-effects hereinafter for the sake of simplicity. When taking the SD-effects into account, the temperature and concentration equations are coupled with each other. Recently, some investigators have conducted numerical and analytical studies to study double-diffusive convection in the presence of SD-effects.

On the literature survey of this subject, Rebi et al. [18] performed numerical and analytical studies to examine thermo-solutal combined convection in a square enclosure filled with binary fluid mixture in the presence of just Soret effect. Later, Nithyadervi and Yang [6] studied the influence of various parameters on double-diffusive convection of water with SD-effects. They found that fluid intensity and heat transfer increase as the Dufuor effect increases. Bhuvaneswari et al. [19] employed numerical simulations to study mixed convection flow with just Soret effect in a two-sided lid-driven cavity. They analyzed the influence of wall movement direction on the transport phenomena, and explored that both of heat and mass transfer would improve if the walls moved in the opposite directions. Wang et al. [8] performed numerical simulations to study double-diffusive convection with SD-effects. Kefayati [20] used the LBM to study double-diffusive natural convection in a square cavity filled with non-Newtonian power-law fluid with SD-effects. Results indicate that the Dufour parameter brings about an enhancement in heat and mass transfer, while Soret parameter just influences the mass transfer. Recently, the same author has utilized the LBM again to do research on double-diffusive convection in an inclined cavity [21]. He infers that the inclination angle is an important factor in influencing heat and mass

transfer. Ren and Chan [22] also used the LBM to investigate double-diffusive convection with Soret and Dufour effects in a rectangular duct. Results again confirm that transport phenomena are affected greatly by Soret and Dufour coefficients' variation.

Although a significant number of studies have been reported with respect to double diffusive convection in square or rectangular enclosure, the non-orthogonal geometry, such as skewed enclosure, has been rarely researched. The constraint due to complex geometry of skewed enclosures makes the research of double-diffusive convection complicated as compared to a square enclosure. The skewed enclosures are the geometries with interesting features and potentials concerning heat and mass transfer performance. They have different heat and mass transfer performances for different skew angles, and they also can even present very different heat transfer behaviours towards either positive or negative skew angles. Further, they have a strong potential to be utilized as the basic structure which leads to high-performance heat transfer elements to be used in multifarious areas such as building applications, solar collectors, electronic thermal control, geothermal applications, etc. [23]. Among the few researchers investigating the convection in non-orthogonal enclosures, Al-Farhany and Turan [24] performed numerical simulations to study double diffusive natural convection inside an inclined rectangular cavity filled with porous media. Results show that there is an inverse relation between the heat transfer and inclination angle. Chamkha et al. [25] studied numerically the natural convection of air in a differentially heated lid-driven parallelogram-shaped enclosure. Their results indicate that Richardson number and inclination angle have significant effects on convective current of heat across the enclosure. Jagadeesha et al. [26] investigated numerically the double diffusive natural convection in an inclined parallelogram-shaped porous enclosure. It has been found that the inclination angle has significant effect on transport phenomena.

After a meticulous survey of the existing literature, it was achieved that less attention has been paid to double-diffusive convection inside a two-sided lid-driven skewed enclosure. In particular, to the author's best knowledge, the problem of double-diffusive natural convection inside a skewed enclosure with SD-effects and in the presence of an external magnetic field has not been reported to date in the literature. Therefore, the core intention of this study is to represent the influence of SD-effects as well as the external magnetic field on double-diffusive convection in a two-sided lid-driven skewed enclosure. Furthermore, the effects of the mentioned features, i.e. Lewis number and buoyancy ratio, on the double-diffusive convection with extra heat and mass diffusions are also examined and discussed to add a view to the problem. On the other hand, various thermal systems are the subject of irreversibility phenomena, which are examined by the entropy generation. The entropy generation is related to heat and mass transfer, chemical reactions, fluid friction, magnetic field, extra heat and mass diffusions, etc. It actually destroys the useful energy of system and causes loss of efficiency. The entropy generation minimization studies have been recognized as optimal design criteria for thermal systems. Thus, the entropy generation analysis of the studied problem is also conducted during this study. The numerical analysis has been performed for a wide range of Hartman number, Lewis number, buoyancy ratio, and skew angle for different sets of Soret and Dufour coefficients. The results are presented in the form of streamlines, isotherms, isoconcentrations, the average Sherwood, and Nusselt numbers. The average entropy generation and entropy generation due to fluid friction and external magnetic field are also reported and discussed.

2. Governing equations and problem formulation

The physical system considered in the current study is depicted in Figure 1. It consists of a skewed enclosure whose bottom wall is along x-axis, and the side walls make angle λ with x-axis. The horizontal walls are maintained at uniform, but different temperatures and concentrations, such that the bottom wall has temperature T_h and concentration C_h, while the top wall has temperature T_l and concentration C_l, where $T_h > T_l$ and $C_h > C_l$. The inclined walls are assumed adiabatic and impermeable. Moreover, the top-cold and bottom-hot walls are assumed to slide uniformly towards the right and left, respectively, at a constant speed, U_0. The fluid (air) is assumed Newtonian, incompressible, and laminar. The fluid properties are assumed constant except for density, which is adopted

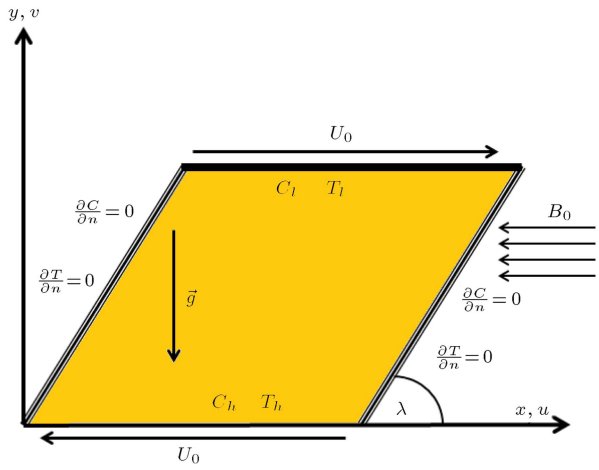

Figure 1. Schematic diagram of the studied problem with boundary conditions in the physical domain.

according to the Boussinesq approximation. The magnetic Reynolds number is assumed small enough, whereby the magnetic induction can be neglected. Meanwhile, viscous dissipation, Hall effect, and heat transfer by radiation are neglected. Under the above assumptions, the dimensionless forms of the governing equations in the binary fluid are expressed as follows:

$$\frac{\partial U}{\partial X}+\frac{\partial V}{\partial Y}=0, \tag{1}$$

$$\frac{\partial U}{\partial \tau}+U\frac{\partial U}{\partial X}+V\frac{\partial U}{\partial Y}=-\frac{\partial P}{\partial X}+\frac{1}{\mathrm{Re}}\left(\frac{\partial^2 U}{\partial X^2}+\frac{\partial^2 U}{\partial Y^2}\right), \tag{2}$$

$$\frac{\partial V}{\partial \tau}+U\frac{\partial V}{\partial X}+V\frac{\partial V}{\partial Y}=-\frac{\partial P}{\partial Y}+\frac{1}{\mathrm{Re}}\left(\frac{\partial^2 U}{\partial X^2}+\frac{\partial^2 V}{\partial Y^2}\right)+\mathrm{Ri}\,(\Theta+B\Phi)-\frac{\mathrm{Ha}^2}{\mathrm{Re}}V, \tag{3}$$

$$\frac{\partial \Theta}{\partial \tau}+U\frac{\partial \Theta}{\partial X}+V\frac{\partial \Theta}{\partial Y}=\frac{1}{\mathrm{Re}\,\mathrm{Pr}}\left[\left(\frac{\partial^2 \Theta}{\partial X^2}+\frac{\partial^2 \Theta}{\partial Y^2}\right)+\mathrm{Df}\left(\frac{\partial^2 \Phi}{\partial X^2}+\frac{\partial^2 \Phi}{\partial Y^2}\right)\right], \tag{4}$$

$$\frac{\partial \Phi}{\partial \tau}+U\frac{\partial \Phi}{\partial X}+V\frac{\partial \Phi}{\partial Y}=\frac{1}{\mathrm{Re}\,\mathrm{Sc}}\left[\left(\frac{\partial^2 \Phi}{\partial X^2}+\frac{\partial^2 \Phi}{\partial Y^2}\right)+\mathrm{Sr}\left(\frac{\partial^2 \Theta}{\partial X^2}+\frac{\partial^2 \Theta}{\partial Y^2}\right)\right]. \tag{5}$$

Herein, the dimensionless variables are defined as follows:

$$(X,Y)=\frac{(x,y)}{L},\quad (U,V)=\frac{(u,v)}{U_0},\quad P=\frac{p}{\rho U_0},$$

$$\tau=\frac{tU_0}{L},\quad \Theta=\frac{T-T_0}{T_h-T_l},\quad \Phi=\frac{C-C_0}{C_h-C_l}.$$

The problem of double-diffusive natural convection with Soret and Dufour effects and subjected to an external magnetic field is characterized by the following dimensionless parameters:

$$\mathrm{Ri}=\frac{\mathrm{Gr}_T}{\mathrm{Re}^2}=\frac{g\beta_T\Delta T L^3/\nu^2}{(U_0L/\nu)^2},$$

$$B=\frac{\beta_C(C_h-C_l)}{\beta_T(T_h-T_l)}=\frac{\mathrm{Gr}_C}{\mathrm{Gr}_T},\quad \mathrm{Le}=\frac{\mathrm{Sc}}{\mathrm{Pr}},$$

$$\mathrm{Df}=\frac{\kappa_{TC}(C_h-C_l)}{\alpha_m(T_h-T_l)},\quad \mathrm{Sr}=\frac{\kappa_{CT}(T_h-T_l)}{D_m(C_h-C_l)},$$

$$\mathrm{Ha}=B_0L\sqrt{\frac{\sigma}{\mu}}.$$

Herein, Gr_C and Gr_T are solutal and thermal Grashof numbers, respectively. Besides, Ri, B, Le, Ha, Sr, and Df are Richardson number, buoyancy ratio, Lewis, number, Hartman numbers, and Soret and Dufour coefficients, respectively. The dimensionless boundary conditions associated with the problem in physical domain are as follows:

$U=1,\ V=0,\ \Theta=\Phi=0$ for $Y=\sin\lambda$,

and $\cos\lambda\le X\le\cos\lambda+1$ (Top wall),

$U=-1,\ V=0,\ \Theta=\Phi=1$ for $Y=0$,

and $0\le X\le 1$ (Bottom wall),

$U=V=0,\ \dfrac{\partial\Theta}{\partial n}=\dfrac{\partial\Phi}{\partial n}=0,$

for $X=Y\cos\lambda\quad(0\le Y\le 1)$

and $0\le Y\le\sin\lambda$ (Left wall),

$U=V=0,\ \dfrac{\partial\Theta}{\partial n}=\dfrac{\partial\Phi}{\partial n}=0,$

for $X=1+Y\cos\lambda\quad(0\le Y\le 1)$

and $0\le Y\le\sin\lambda$ (Right wall),

where n is the normal displacement with respect to the left- and right-side walls. The skewed enclosure in the physical domain in x,y-plane is transformed into an orthogonal system in the computational domain by the co-ordinate transformations proposed before by Nayak et al. [27]. In this way, independent variables x,y in the physical domain are transformed into independent variables ζ, and η in the computational domain by the following relation:

$$\zeta=x-y\cot\lambda,\quad \eta=y/\sin\lambda. \tag{6}$$

Under this transformation, the non-dimensional governing equations in the computational domain can be written as follows:

$$\frac{\partial}{\partial\zeta}(U-V\cot\lambda)+\frac{\partial}{\partial\eta}\left(\frac{V}{\sin\lambda}\right)=0, \tag{7}$$

$$\frac{\partial U}{\partial\tau}+\frac{\partial}{\partial\zeta}(UU)-\cot\lambda\frac{\partial}{\partial\zeta}(UV)+\frac{1}{\sin\lambda}\frac{\partial}{\partial\eta}(UV)=-\frac{\partial P}{\partial\zeta}\frac{a}{\mathrm{Re}}\left(\frac{\partial^2 U}{\partial\zeta^2}+\frac{\partial^2 U}{\partial\eta^2}-2c\frac{\partial^2 U}{\partial\zeta\partial\eta}\right), \tag{8}$$

$$\frac{\partial V}{\partial \tau}+\frac{\partial}{\partial \zeta}(UV)-\cot\lambda\frac{\partial}{\partial \zeta}(UV)+\frac{1}{\sin\lambda}\frac{\partial}{\partial \eta}(VV)$$
$$=-\frac{1}{\sin\lambda}\frac{\partial P}{\partial \eta}+\cot\lambda\frac{\partial P}{\partial \zeta}\frac{a}{\mathrm{Re}}\left(\frac{\partial^2 V}{\partial \zeta^2}+\frac{\partial^2 V}{\partial \eta^2}-2c\frac{\partial^2 V}{\partial \zeta\partial \eta}\right)+\mathrm{Ri}(\Theta+B\Phi)-\frac{\mathrm{Ha}^2}{\mathrm{Re}^2}V, \quad (9)$$

$$\frac{\partial \Theta}{\partial \tau}+\frac{\partial}{\partial \zeta}(U\Theta)-\cot\lambda\frac{\partial}{\partial \zeta}(V\Theta)+\frac{1}{\sin\lambda}\frac{\partial}{\partial \eta}(V\Theta)$$
$$=\frac{a}{\mathrm{Re}\,\mathrm{Pr}}\left[\left(\frac{\partial^2 \Theta}{\partial \zeta^2}+\frac{\partial^2 \Theta}{\partial \eta^2}-2c\frac{\partial^2 \Theta}{\partial \zeta\partial \eta}\right)+\mathrm{Df}\left(\frac{\partial^2 \Phi}{\partial \zeta^2}+\frac{\partial^2 \Phi}{\partial \eta^2}-2c\frac{\partial^2 \Phi}{\partial \zeta\partial \eta}\right)\right], \quad (10)$$

$$\frac{\partial \Phi}{\partial \tau}+\frac{\partial}{\partial \zeta}(U\Phi)-\cot\lambda\frac{\partial}{\partial \zeta}(V\Phi)+\frac{1}{\sin\lambda}\frac{\partial}{\partial \eta}(V\Phi)$$
$$=\frac{a}{\mathrm{Re}\,\mathrm{Sc}}\left[\left(\frac{\partial^2 \Phi}{\partial \zeta^2}+\frac{\partial^2 \Phi}{\partial \eta^2}-2c\frac{\partial^2 \Phi}{\partial \zeta\partial \eta}\right)+\mathrm{Sr}\left(\frac{\partial^2 \Theta}{\partial \zeta^2}+\frac{\partial^2 \Theta}{\partial \eta^2}-2c\frac{\partial^2 \Theta}{\partial \zeta\partial \eta}\right)\right], \quad (11)$$

where $a = coesc^2\lambda$ and $c = \cos\lambda$. The appropriate boundary conditions in the computational domain are given as follows:

$$U=1,\quad V=0,\quad \Theta=\Phi=0,\quad \text{at}\quad \eta=1,$$

$$U=-1,\quad V=0,\quad \Theta=\Phi=1,\quad \text{at}\quad \eta=0,$$

$$U=V=0,\quad \frac{\partial \Theta}{\partial \zeta}=\cos\lambda\frac{\partial \Theta}{\partial \eta},\quad \frac{\partial \Phi}{\partial \zeta}=\cos\lambda\frac{\partial \Phi}{\partial \eta},\quad \text{at}\quad \zeta=0,$$

$$U=V=0,\quad \frac{\partial \Theta}{\partial \zeta}=\cos\lambda\frac{\partial \Theta}{\partial \eta},\quad \frac{\partial \Phi}{\partial \zeta}=\cos\lambda\frac{\partial \Phi}{\partial \eta},\quad \text{at}\quad \zeta=1.$$

To evaluate the heat and mass transfer within the skewed enclosure, the average Nusselt and Sherwood numbers along the horizontal wall with maximum temperature and concentration are examined. For this purpose, the local Nusselt and Sherwood numbers are determined as follows:

$$\mathrm{Nu}=\left(-\frac{\partial \Theta}{\partial \eta}\right)_{\eta=0}+\mathrm{Df}\left(-\frac{\partial \Phi}{\partial \eta}\right)_{\eta=0},$$

$$\mathrm{Sh}=\left(-\frac{\partial \Phi}{\partial \eta}\right)_{\eta=0}+\mathrm{Sr}\left(-\frac{\partial \Theta}{\partial \eta}\right)_{\eta=0}. \quad (12)$$

The average Nusselt and Sherwood numbers along the hot wall are then calculated by integrating the local Nusselt and Sherwood numbers as follows:

$$\overline{\mathrm{Nu}}=\int_0^1 \mathrm{Nu}d\zeta,\quad \overline{\mathrm{Sh}}=\int_0^1 \mathrm{Sh}d\zeta. \quad (13)$$

In order to quantify the effect of external magnetic field on the transport phenomena, the following average Nusselt and Sherwood numbers are also defined and calculated as follows:

$$\overline{\mathrm{Nu}}^{**}=\frac{\overline{\mathrm{Nu}}(\mathrm{Ha})}{\overline{\mathrm{Nu}}(\mathrm{Ha}=0)},\quad \overline{\mathrm{Sh}}^{**}=\frac{\overline{Sh}(\mathrm{Ha})}{\overline{Sh}(\mathrm{Ha}=0)}. \quad (14)$$

The influence of key parameters on the total kinetic energy is also investigated in this study. The total kinetic energy is calculated using an expression introduced by Goyan as follows [28]:

$$E=\sqrt{\sum_{(i,j)=(1,1)}^{(n_x,n_y)}\left[\left(U_{i,j}^2\right)+\left(V_{i,j}^2\right)\right]}. \quad (15)$$

It should be noted that the total kinetic energy is calculated with respect to the studied grid, and then it is averaged during the final 1000 time steps of simulations. The local entropy generation of double-diffusive convection with magnetic effect can be written as follows:

$$S_{gen}=S_F+S_T+S_C+S_B, \quad (16)$$

where S_F, S_T, S_C, and S_B are the local entropy generation due to fluid friction irreversibility, heat transfer irreversibility, mass transfer irreversibility, and magnetic field effect, respectively. Those irreversibilities in the physical domain are defined as follows [29,30]:

$$S_F=\frac{\mu}{T_0}\left[2\left(\frac{\partial u}{\partial x}\right)^2+2\left(\frac{\partial v}{\partial y}\right)^2+\left(\frac{\partial u}{\partial x}+\frac{\partial v}{\partial y}\right)^2\right], \quad (17)$$

$$S_T=\frac{k}{{T_0}^2}\left[\left(\frac{\partial T}{\partial x}\right)^2+\left(\frac{\partial T}{\partial y}\right)^2\right], \quad (18)$$

$$S_C=\frac{RD_m}{C_0}\left[\left(\frac{\partial C}{\partial x}\right)^2+\left(\frac{\partial C}{\partial y}\right)^2\right]+\frac{RD_m}{T_0}\left[\left(\frac{\partial C}{\partial x}\right)\left(\frac{\partial T}{\partial x}\right)+\left(\frac{\partial C}{\partial y}\right)\left(\frac{\partial T}{\partial y}\right)\right], \quad (19)$$

$$S_B=\frac{\sigma B_0^2}{T_0}v^2. \quad (20)$$

T_0 and C_0 are the bulk temperature and bulk concentration, receptively ($T_0 = \frac{T_h+T_l}{2}$, and $C_0 = \frac{C_h+C_l}{2}$). Meanwhile, k, μ, and σ are thermal conductivity, dynamic viscosity, and electrical conductivity, respectively, while R is the gas constant. The dimensionless form of various terms of the entropy generation after being transformed into the computational domain by utilizing Eq. (6) can be written as follows:

$$S_F = \chi_I \left[2\left(\left(\frac{\partial U}{\partial \zeta}\right)^2 + \left(-\frac{\partial V}{\partial \zeta}\cot\lambda + \frac{\partial V}{\partial \eta}\cos ec\lambda \right)^2 \right) + \left(\frac{\partial}{\partial \zeta}(V - U\cot\lambda) + \frac{\partial U}{\partial \eta}\cos ec\lambda \right)^2 \right], \quad (21)$$

$$S_T = \left[\left(\frac{\partial \Theta}{\partial \zeta}\right)^2 + \left(-\frac{\partial \Theta}{\partial \zeta}\cot\lambda + \frac{\partial \Theta}{\partial \eta}\cos ec\lambda \right)^2 \right], \quad (22)$$

$$S_C = \chi_{II} \left[\left(\frac{\partial \Phi}{\partial \zeta}\right)^2 + \left(-\frac{\partial \Phi}{\partial \zeta}\cot\lambda + \frac{\partial \Phi}{\partial \eta}\cos ec\lambda \right)^2 \right] + \chi_{III} \left[\left(\frac{\partial \Theta}{\partial \zeta}\right)\left(\frac{\partial \Phi}{\partial \zeta}\right) + \left(-\frac{\partial \Theta}{\partial \zeta}\cot\lambda + \frac{\partial \Theta}{\partial \eta}\cos ec\lambda \right)\left(-\frac{\partial \Phi}{\partial \zeta}\cot\lambda + \frac{\partial \Phi}{\partial \eta}\cos ec\lambda \right) \right], \quad (23)$$

$$S_B = \chi_I \mathrm{Ha}^2 V^2, \quad (24)$$

where:

$$\chi_I = \frac{\mu T_0}{k}\left(\frac{U_0}{T_h - T_l}\right)^2 = \mathrm{Br} T_0/\Delta T,$$

$$\chi_{II} = \frac{R D_m T_0^2}{k C_0}\left(\frac{C_h - C_l}{T_h - T_l}\right)^2,$$

$$\chi_{III} = \frac{R D_m T_0}{k C_0}\left(\frac{C_h - C_l}{T_h - T_l}\right).$$

Br = PrEc is the Brinkman number, where Ec = $\frac{U_0^2}{C_P \Delta T}$ is the Eckert number [29]. The average entropy generation is then given as follows:

$$\overline{S_{avg}} = \int_0^1 \int_0^1 S_{gen} d\zeta d\eta. \quad (25)$$

To examine the contribution of irreversibility due to thermal and solutal effects in the entropy generation, the following ratios are reported, respectively, as follows:

$$\overline{S_T}^{\dagger} = \int_0^1 \int_0^1 \left(\frac{S_T}{S_{gen}}\right) d\zeta d\eta, \quad \overline{S_C}^{\dagger} = \int_0^1 \int_0^1 \left(\frac{S_C}{S_{gen}}\right) d\zeta d\eta. \quad (26)$$

3. Numerical solution

First, it should be reminded that the governing equations in the orthogonal computational domain are numerically solved in this study. The dimensionless unsteady governing equations, i.e. Eqs. (7)-(11), are discretized by the finite volume method developed by Patankar [31]. The convection term discretized using the QUICK scheme, while second-order Adams-Bashforth explicit scheme is implemented for the unsteady term. The SIMPLE algorithm is then employed to solve the discretized equations. The effect of concentration is also taken into account using pressure correction method to obtain the real velocity field. $\overline{\mathrm{Nu}}$ and $\overline{\mathrm{Sh}}$ are calculated using Simpson's integration rule. However, the used numerical method had to be validated against previously published results to check the code credibility. The validation procedure, convergence and independency tests are presented in the following.

3.1. Convergence criteria

The time step is chosen as $\Delta\tau = 0.001$ which was used before in the study of Al-Amiri et al. [9]. Meanwhile, the convergence of the numerical results is also employed, and the following criterion on each time step is satisfied:

$$\sum_{i,j} \left| \Pi_{i,j}^q - \Pi_{i,j}^{q-1} \right| \leq 10^{-6},$$

where generic variable Π represents the sets of U, V, Θ, or Φ, and q indicates the iteration number in one time step. The subscript sequence (i, j) represents the space coordinates of the grid node.

3.2. Grid independency test

The grid independency test study is performed to find the proper grid size. For this, the simulations were performed on three different uniform grids, namely 110×110, 150×150, and 180×180, for a typical case dealing with Re = 100 and Ri = 0.01. The difference between the results obtained for various grid sizes was detected to be less than 0.3%. For the sake of accuracy required within a reasonable amount of computation time, the grid of 150×150 nodes is utilized for all computations reported in this study.

3.3. Model validation

To establish the code credibility, the present numerical model had to check against previously published solutions. Most of the previous publications have studied double-diffusive convection without SD-effects. Thus, numerical solutions were produced for a case with Sr = Df = 0. Screibr and Keller [32] and Al-Amiri et al. [9] carried out numerical simulations to study double-diffusive convection in a driven cavity with one moving lid. The stream function values at the primary vortex

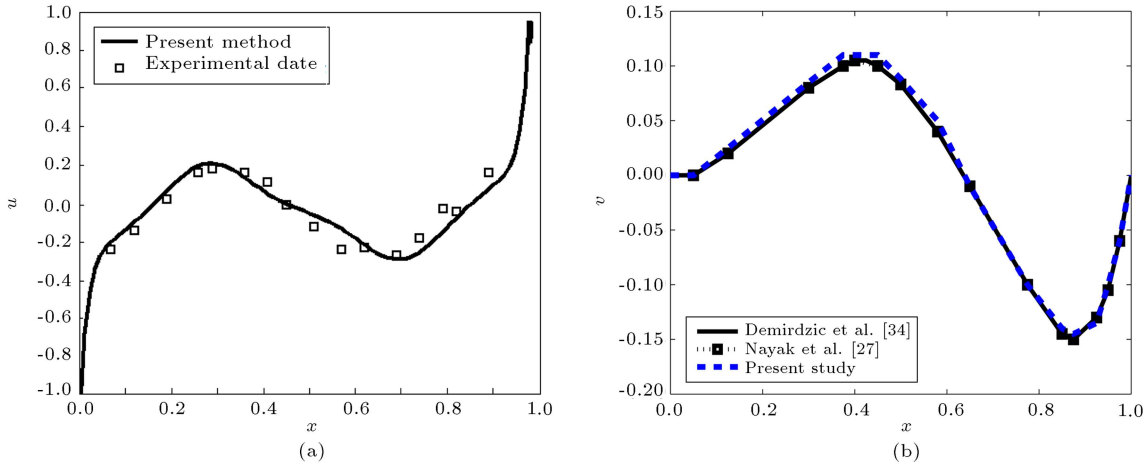

Figure 2. (a) The comparison of the present results for u-velocity profile with the experimental results due to Kuhlmann et al. [33]. (b) The comparison of the present results for v-velocity profile with the numerical results due to Demirdzic et al. [34] and Nayak et al. [27], when Re = 100 and $\lambda = 45°$ for pure fluid.

Table 1. Comparison of primary vortex stream functions, $|\psi_{\text{Max}}|$, obtained from the present method and previously published results.

Re	Present work	Al-Amiri et al. [9]	Screiber & Keller [32]
100	−0.1031	−0.1033	−0.1033
400	−0.1132	−0.1139	−0.1138

location calculated by the mentioned authors and those calculated by the presented method in this study are compared in Table 1 for two Reynolds numbers. Good agreement is found between the results. The present method is then validated against data results measured by Kuhlmann et al. [33]. They investigated experimentally the mixed convection in a two-sided lid-driven cavity. Hence, the presented method was performed in an identical flow geometry, when horizontal walls are moving with the same velocities, yet in the opposite directions. Buoyancy ratio, B, was also set to zero to simulate mixed convection in the absence of the concentration gradient. The obtained results from the present method and experimental data are compared in Figure 2(a). It can be seen that the calculated results are in good agreement with the measured data. A third test concerning the vertical velocity along the horizontal central line obtained by the method developed in this study by Demirdciz et al. [34] and Nayak et al. [27] was conducted for a natural convection in a lid-driven skewed cavity with $\lambda = 45°$; the data results are compared in Figure 2(b). As one can remark, excellent agreement is observed.

4. Results and discussion

A computational analysis has been conducted on the unsteady thermo-solutal combined natural convection in various skewed two-sided lid-driven enclosures in the presence of an uniform magnetic field and with Soret and Dufour effects, simultaneously. Simulations are performed in six skewed cavities with $\lambda = 15°, 30°, 45°, 60°, 75°$, and $90°$. The key parameters, namely Hartman number, Lewis number, Buoyancy ratio, and Dufour coefficient, vary in almost wide ranges, when $0 \leq \text{Ha} \leq 30$, $1 \leq \text{Le} \leq 50$, $-10 \leq B \leq 10$, and $0 \leq \text{Df} \leq 7$, respectively. The remaining parameters are fixed at Reynolds number (Re = 100), Grashof number ($\text{Gr} = 10^5$), Prandtl number (Pr = 0.71), and Soret coefficient (Sr = 0.25). The parametric study is focused on the effects of magnetic field strength, ratio of thermal to mass diffusivity, ratio of thermal to mass buoyancy forces, and extra heat diffusion on the dynamic, thermal and solutal fields as well as the heat and mass transfer. Moreover, the influences of key parameters on the total kinetic energy, absolute value of the stream function at primary vortex as well as the entropy generation are analyzed and discussed. It should be noted that fluid flow as well as the isotherm and isoconcentration patterns are presented in skewed enclosures with $\lambda = 30°, 45°, 60°$, and $90°$ for the sake of brevity.

4.1. Influence of Hartman number

Figure 3 depicts the influence of Hartman number on flow fields and isotherm patterns. The variations of isoconcentrations are found to be qualitatively similar to the isotherms, not elaborated here for the sake of brevity. It should be noticed that Lewis number, buoyancy ratio, Soret and Dufour coefficients are kept constant during the section, whereby $\text{Le} = B = 1$ and $\text{Sr} = \text{Df} = 0.25$; therefore, similar obtained patterns for thermal and solutal fields seem to be logical. In fact, the hot fluid rises up from the heated bottom wall and the cold fluid goes down along the

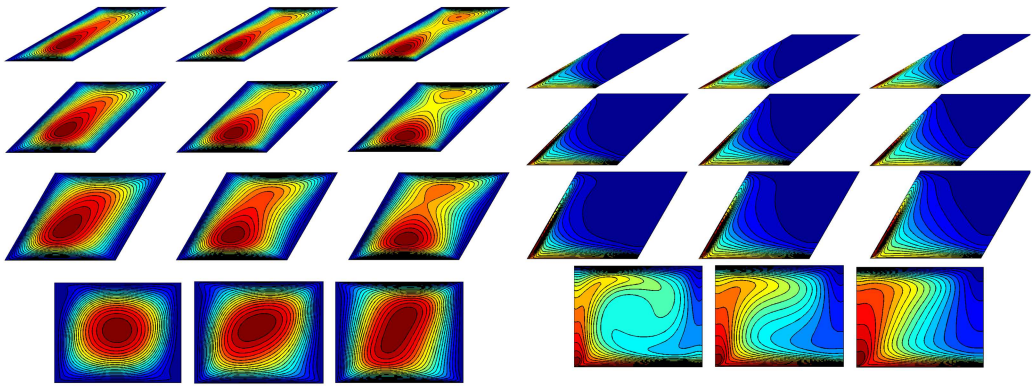

Figure 3. Effect of Hartman number on (a) streamlines and (b) isotherms in four skewed enclosures with $\lambda = 30°, 45°, 60°$, and $90°$, while Ha = 0, 10, and 30 in the first, second, and third columns, respectively, and Ri = 10, Le = B = 1, and Df = Sr = 0.25 in all the cases.

cold cross wall because of imposed temperature and concentration gradients between the horizontal walls on the one side and the thermal and solutal buoyancies on the other side. Besides, the flow fields have been affected greatly by the movement of the lids, due to which streamlines are stretched towards the right and left near the moving top and bottom lids, respectively. It can be seen that, at skew angle, $\lambda = 90°$, the primary vortex is symmetric about the central line of the enclosure. In addition, the thickness of the boundary layer in the vicinity of the moving lids enhances as the Hartman number increases. This fact represents either the augmentation of shear forces or attenuation of buoyancy effects in those regions with an enhancement of Hartman number. Lorentz force has a tendency to slow down the convection flow field within the enclosure. The suppression effect of external magnetic field on buoyancy forces has been reported by many previous investigators, e.g. Borhan Uddin et al. [17], and Ghaffarpasand [35].

Figure 3(a) also shows that the size of the primary vortex is enhanced with further increase of skew angle. The effective area of the skewed enclosures enhances as the skew angle increases. In skewed enclosures with larger effective areas, fluid flow as well as the solutal and thermal fields develop greatly, whereby the size of the primary vortex is enhanced with further increasing of skew angle as can be observed in Figure 3(a). This fact was also observed before in the study of Erturk and Dursun [36]. It can also be seen that the primary vortex in cases with $\lambda < 90°$ starts to divide into two vortices with further increase of Hartman number. Those vortices are formed by the shear forces induced by the lids movement in the opposite direction. The sizes of those vortices are augmented by increasing the suppression effect of Lorentz force against buoyancy forces.

Figure 3(b) shows the influence of skew angle and external magnetic field on the isotherm patterns. First, it can be seen that the isotherms near the hot wall are approximately parallel to each other in all skewed enclosures. This indicates that the conduction is the dominant mechanism of heat transfer near the hot wall. The distortion of isotherm lines at the core region represents the convective current of heat across the enclosure. As the Hartman number increases, the isotherms become parallel to the horizontal hot walls even in the core region. This implies that Lorentz force has a suppression effect on the convective heat transfer.

The external magnetic field also affects the fluid intensity as well as the total kinetic energy of the double diffusive natural convection within the skewed enclosure. To analyze this feature, the variations of $|\psi_{\text{Max}}|$ and $\overline{E}$ as a function of skew angle for various Hartman numbers are illustrated in Figure 4(a) and (b), respectively. The suppression effect of magnetic field on the fluid intensity and total kinetic energy can also be observed here. Nevertheless, the influence of Hartman number on both of them are augmented with increasing skew angle of the skewed enclosure. To evaluate the heat transfer characteristics, the variation of average Nusselt number as a function of skew angle for various Hartman numbers is depicted in Figure 4(c). It should be noted that the extra cases, including double diffusive natural convection in lid-driven (one-sided) skewed enclosures, in the absence of external magnetic field and SD-effects is also presented here to help better understand. It can be seen that $\overline{\text{Nu}}$ in a lid-driven skewed enclosure without an external magnetic field is improved with increasing skew angle of enclosure. This result resembles those of Hussein and Hussain [37] and Nayak et al. [27] for a lid-drive skewed cavity filled with a pure fluid (pure air with Pr = 0.71). Figure 4(c) also shows that although $\overline{\text{Nu}}$ in the two-sided enclosures is generally larger than that in the one-sided enclosures; however, the variations of those as a function of λ are not completely similar. The moving of the bottom lid in two-sided lid-driven

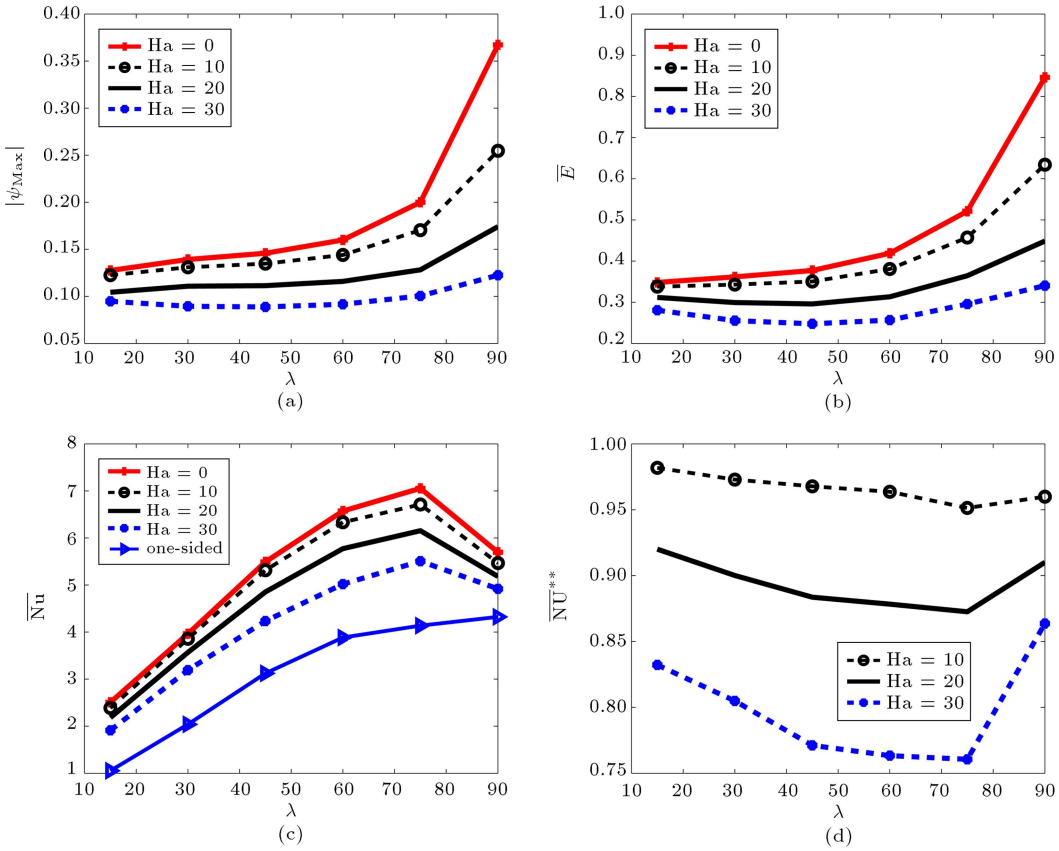

Figure 4. The variations of (a) the absolute value of stream function at primary vortex, (b) the total kinetic energy, (c) the average Nusselt number, and (d) $\overline{Nu}^{**}$ value as a function of skew angle for various Hartman numbers, while Ri = 10, Le = B = 1, and Df = Sr = 0.25.

skewed enclosures may push the flow to penetrate much deeper into the enclosure; as a result, two-sided skewed enclosures have larger $\overline{Nu}$ values than one-sided lid-driven skewed enclosures.

It can be seen that the inflection points exist on $\lambda = 75°$, whereby the general growing trend of $\overline{Nu}$ values due to the skew angle enhancement is changed at that point. This inflection may be due to the increase of the suppression effect of Lorentz force and the convective heat transfer with further increase of λ from 75° to 90°. However, it is obvious that the convective heat transfer, $\overline{Nu}$ values, is reduced with the further increase of Ha values due to the suppression effect of Lorentz force against the thermal buoyancy forces. The variation in rates of average Nusselt number due to applying external magnetic field, $\overline{Nu}^{**}$, as a function of skew angle for various Hartman numbers is illustrated in Figure 4(d). The suppression effect of Lorentz force is also well observed here, whereby all of $\overline{Nu}^{**}$ values are smaller than unity, and the cases with larger Hartman numbers have smaller $\overline{Nu}^{**}$ values.

Figure 5 represents the influence of Hartman number on the entropy generation and various fluid irreversibilities. As can be observed in Figure 5(a), the total entropy generation reduces as either skew angle or Hartman number reduces. The effective area of the skewed enclosures enhances as the skew angle value increases, due to which the local entropy generation and average entropy generation reduce. Hence, the trend of the average entropy generation is opposite to that of the average Nusselt number (Figure 4(c)). This feature was also observed before in the study of Nayak et al. [27]. It can also be seen that the average entropy generation reduces as the Hartman number increases. This fact can be attributed to the suppression effect of Lorenz force which reduces greatly the fluid intensity/friction across the skewed enclosure.

Figuer 5(b) shows that the fluid irreversibility due to the magnetic effect increases as either skew angle or Hartman number increases. The enhancement of $\overline{S_B}$ values with Hartman number is due to the straight relation of fluid irreversibility due to magnetic effect and Ha value (see Eq. (23)). Nevertheless, it can be seen that the influence of magnetic field on $\overline{S_B}$ values is augmented by increasing the effective area of the skewed enclosure. Figure 5(c) represents the variation of fluid friction irreversibility across the skewed enclosures. As the Hartman number enhances, the fluid intensity reduces which results in the reduction of $\overline{S_F}$ values. Meanwhile, reducing the effective area can de-

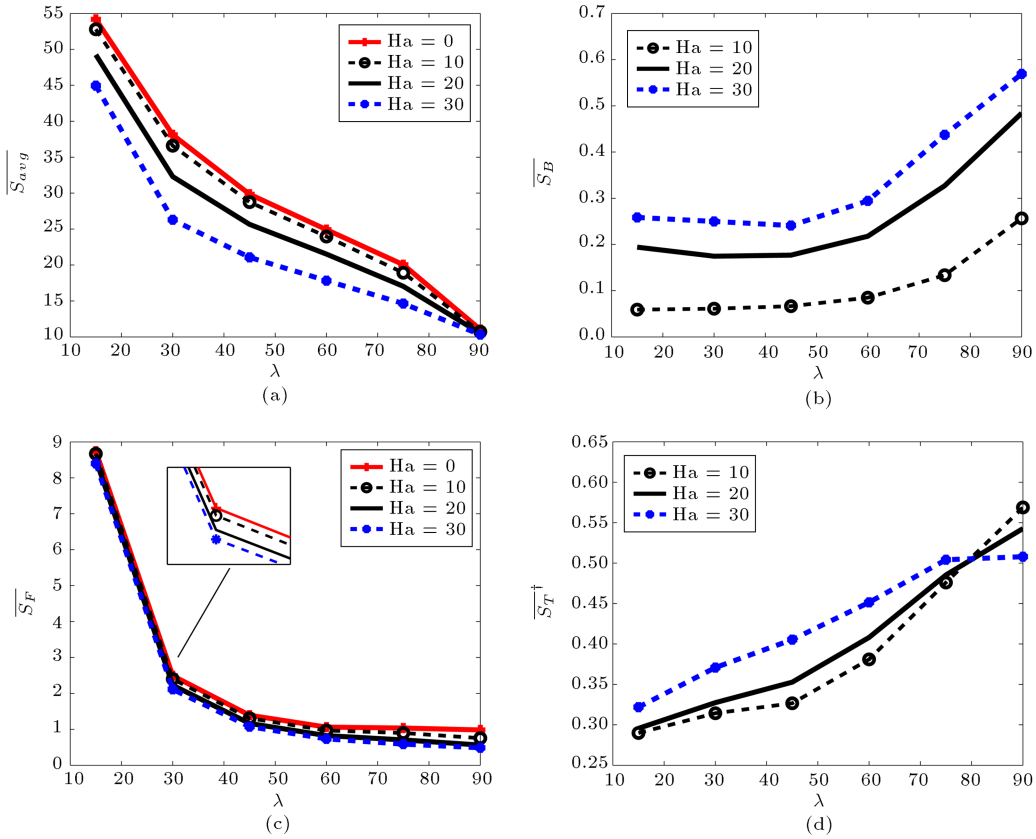

Figure 5. The variations of (a) the absolute value of stream function at primary vortex, (b) the total kinetic energy, (c) the average Nusselt number, and (d) $\overline{S_T}^{\dagger}$ value as a function of skew angle for various Hartman numbers, while Ri = 10, Le = B = 1, and Df = Sr = 0.25.

crease the local entropy generation due to fluid friction and $\overline{S_F}$ values. The contribution of irreversibility due to heat transfer in the total entropy generation, $\overline{S_T}^{\dagger}$, as a function of skew angle and for various non-zero Hartman numbers is illustrated in Figure 5(d). It can be seen that $\overline{S_T}^{\dagger}$ values enhance as the effective area of the skewed enclosure increases. It may be noted that with the increase of effective area, the buoyancy effect enhances for which the irreversibility increases due to heat transfer, $\overline{S_T}^{\dagger}$ value. However, in skewed enclosures, $\lambda \neq 90°$, increasing suppression effect of Lorentz force attenuates the irreversibility due to fluid friction, and so increases $\overline{S_T}^{\dagger}$ value. In contrast, in square enclosures where the convective current of heat has developed greatly, increasing Hartman number attenuates thermal effects, and so reduces $\overline{S_T}^{\dagger}$ value.

4.2. Influence of Lewis number

The influences of Lewis number on the streamlines and isotherms of combined thermo-solutal natural convection inside a two-sided lid-driven skewed enclosure and in the presence of a constant magnetic field (Ha = 10) with SD-effects (Sr = Df = 0.25) are illustrated in Figure 6. Lewis number is the ratio of thermal to mass diffusivity and reflects the mass transfer exchange between the two zones with different concentrations. Figure 6 exhibits that the influence of Lewis number on the streamlines and isotherms seems to be insignificant. The similarity was explored before in the studies of Al-Amiri et al. [9] and Teamah and El-Maghlaney [38], where the combined thermo-solutal convection without external magnetic field and SD-effects inside a square enclosure was studied.

The influences of Lewis number on fluid intensity and total kinetic energy are depicted in Figure 7(a) and (b), respectively. It can be seen that the influence of Lewis number on both $|\psi_{\mathrm{Max}}|$ and $\overline{E}$ values seems to be negligible. Nevertheless, both of them are reduced slightly with increasing Lewis number. To better evaluate the heat transfer across the enclosure, the variations of the average Nusselt number as a function of λ for various Lewis numbers and for the cases with and without SD-effects are illustrated in Figure 8(a) and (b), respectively. The figures demonstrate that the heat transfer across the enclosure in cases with SD-effects is reduced with further increasing of Lewis number, while the opposite is observed in cases without SD-effects. It is worthwhile to note that the variation of the average Nusselt number as a function of Lewis

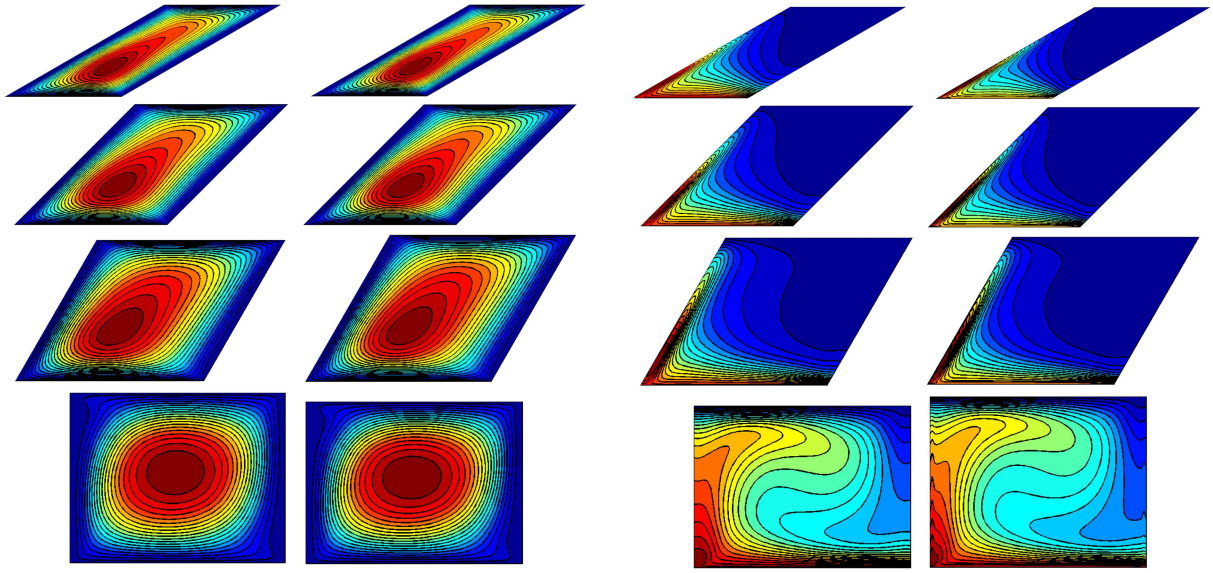

(a) (b)

Figure 6. Effect of Lewis number on (a) streamlines and (b) isotherms in four skewed enclosures with $\lambda = 30°, 45°, 60°$, and $90°$, while Le = 1 and 50 in left and right columns, respectively, and Ri = 10, $B = 1$, Ha = 10, and Df = Sr = 0.25 in all the cases.

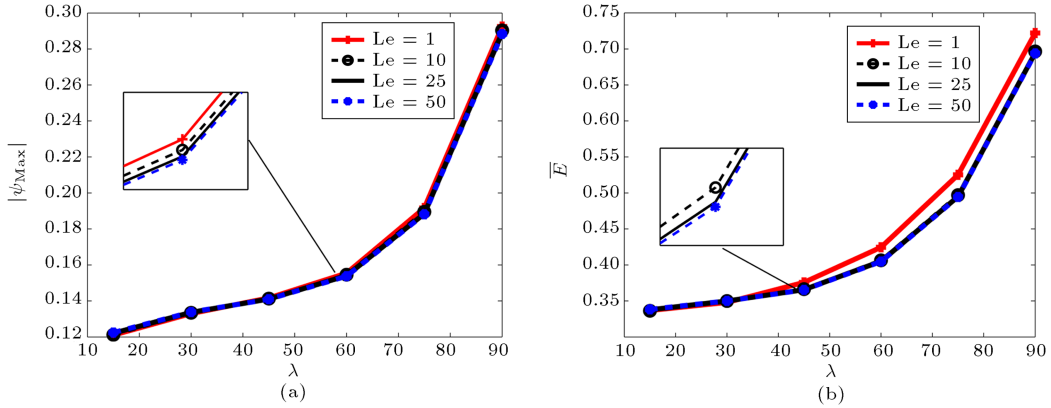

Figure 7. The variations of (a) the absolute value of stream function at primary vortex and (b) the total kinetic energy as a function of skew angle for various Lewis numbers, while Ri = 10, $B = 1$, Ha = 10, and Df = Sr = 0.25.

number in square enclosures ($\lambda = 90°$) without SD-effects (Figure 8(b)) is similar to the obtained results of Al-Amiri et al. [9]. The reduction of Lewis number corresponds with either attenuation of thermal diffusivity or augmentation of mass diffusivity. The mass transfer and also concentration gradient across the enclosure enhance as the mass diffusivity increases. According to Eq. (12), increasing concentration gradient in cases with SD-effects improves the heat transfer across the enclosure, whereby $\overline{Nu}$ is a reducing function of Lewis number in those cases. The variations of $\overline{Sh}$ for cases with and without SD-effects are presented in Figure 8(c) and (d), respectively. As can be seen the presence of SD-effects did not influence the role of Lewis number in the mass transfer variation across the skewed enclosure, whereby the mass transfer is reduced with the rise of Lewis number in both cases. The average Sherwood number also achieves its maximum value in the cases with the largest effective area and the largest skew angle. In fact, the convective current of mass is developed greatly in skewed enclosures with larger effective areas, whereby $\overline{Sh}$ is an increasing function of λ.

The variations of $\overline{Nu}^{**}$ and $\overline{Sh}^{**}$ values as a function of skew angle for cases with SD-effects are illustrated in Figure 8(e) and (f), respectively. First, in accordance to the range of variations, it appears that the influence of Lewis number on both of $\overline{Nu}^{**}$ and $\overline{Sh}^{**}$ values is insignificant. Nevertheless, it can be seen that $\overline{Nu}^{**}$ values are smaller than unity, while the opposite is true for $\overline{Sh}^{**}$ values. In other words, although the external magnetic field reduces heat transfer and suppression effect of Lorentz force, it could increase simultaneously mass transfer across the skewed en-

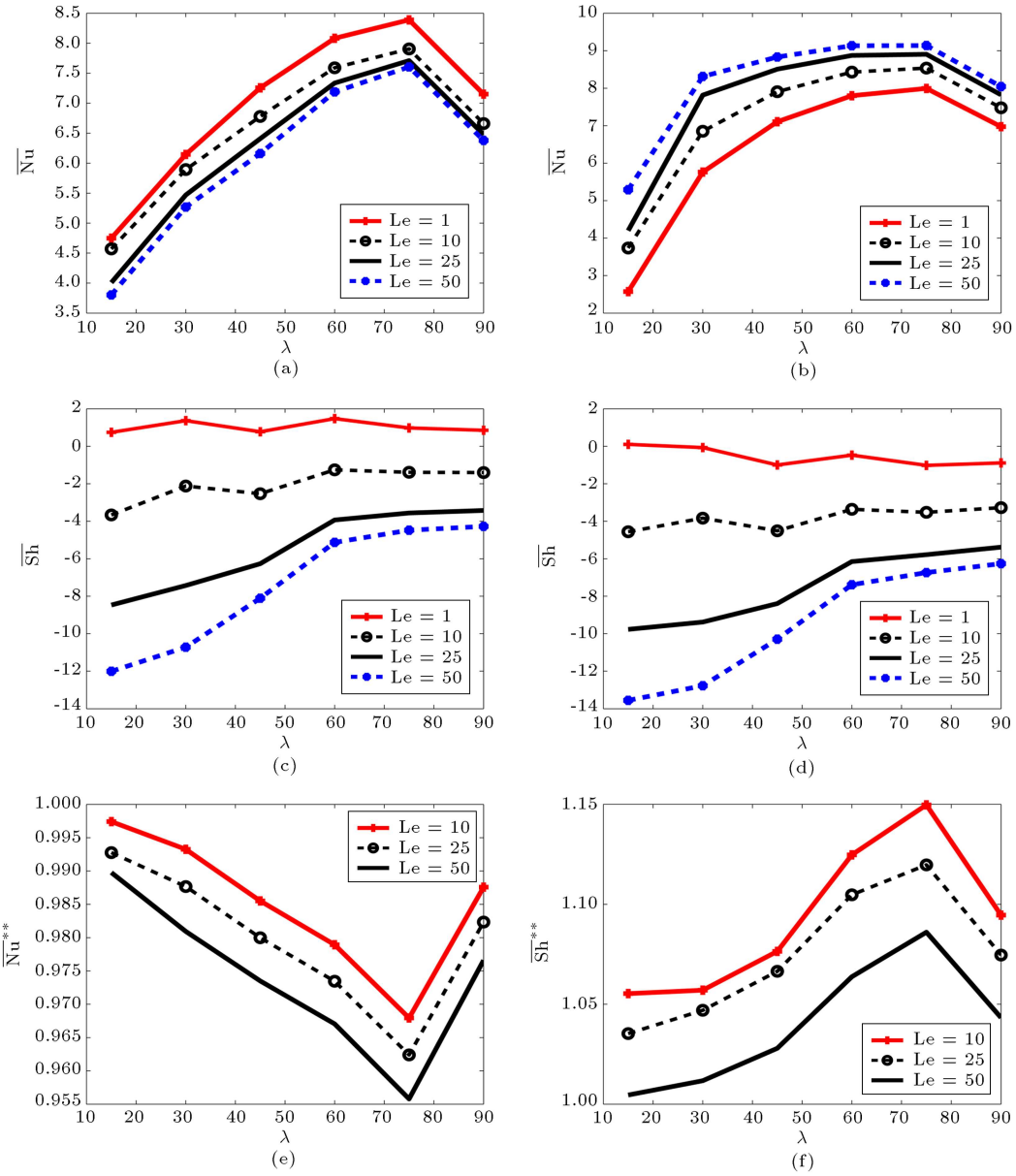

Figure 8. The variations of (a) the average Nusselt number with SD-effects and (b) the average Nusselt number without SD-effects, (c) the average Sherwood number with SD-effects, (d) the average Sherwood number without SD-effects, (e) $\overline{\mathrm{Nu}}^{**}$ value, and (f) $\overline{\mathrm{Sh}}^{**}$ value as a function of skew angle for various Lewis numbers, while Ri = 10, $B = 1$, Ha = 10, and Df = Sr = 0.25.

closures. Meanwhile, the cases with larger Lewis numbers have smaller $\overline{\mathrm{Nu}}^{**}$ and larger $\overline{\mathrm{Sh}}^{**}$ values. The enhancement of Lewis number increases the thermal diffusivity, thus increasing the suppression effect of Lorentz force against the thermal effect across the skewed enclosure. On the other hand, reducing thermal buoyancy forces due to applying external magnetic field cause an enhancement in solutal effects, whereby $\overline{\mathrm{Sh}}^{**}$ values are larger than unity. The reduction of Lewis number corresponds to an enhancement of mass diffusivity, and so the cases with smaller Lewis numbers have larger $\overline{\mathrm{Sh}}^{**}$ values.

The influences of Lewis number on the entropy generation and various fluid irreversibilities are presented in Figure 9. As can be observed in Figure 9(a), the average entropy generation increases with further enhancement of Lewis number. The enhancement of thermal diffusion within the skewed enclosure improves the local fluid irreversibilities, and so increases the average entropy generation. Meanwhile, the influence of Lewis number on the entropy generation is pronounced by reducing skew angle. Figure 9(b) clearly shows that the effect of Lewis number on the fluid irreversibility due to fluid friction can be ignored. Nevertheless, a partial enhancement in $\overline{S_F}$ values due to Lewis number reduction is observed. Figure 9(c) and (d)

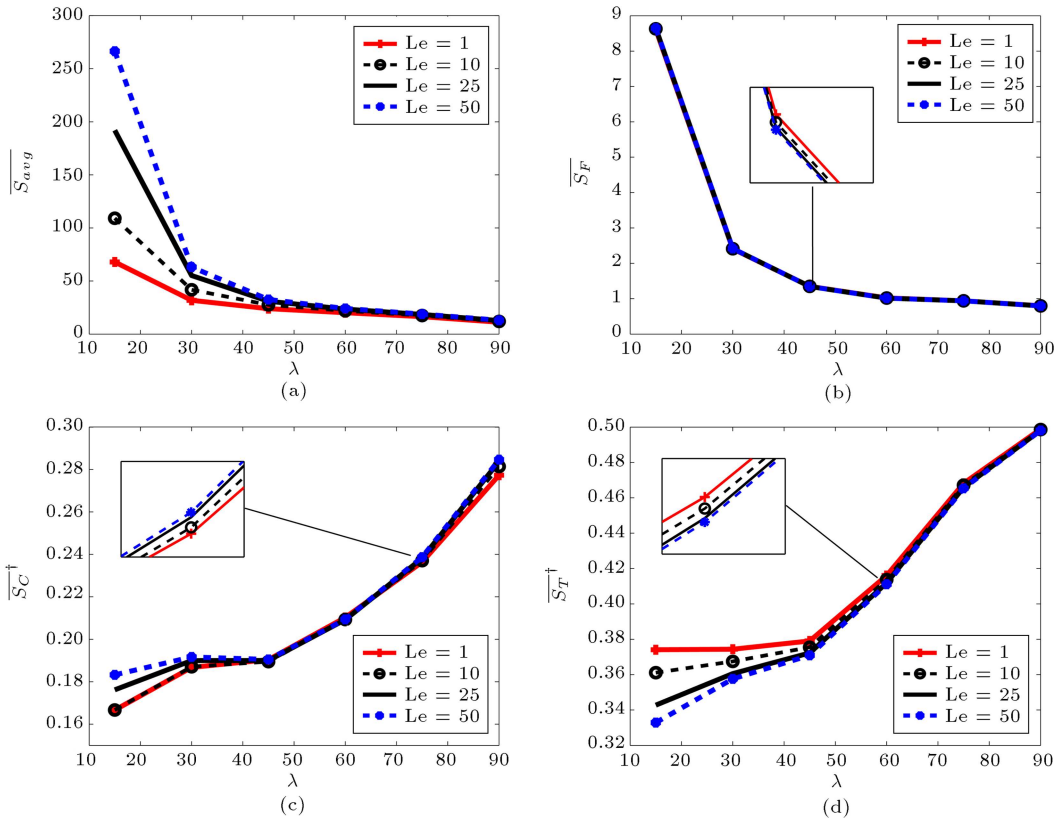

Figure 9. The variations of (a) the average entropy generation, (b) the average entropy generation due to fluid friction irreversibility, (c) $\overline{S_C}^{\dagger}$, and (d) $\overline{S_T}^{\dagger}$ value as a function of skew angle for various Lewis numbers, while Ri = 10, $B = 1$, Ha = 10, and Df = Sr = 0.25.

demonstrate that the influences of Lewis number on irreversibility due to heat and mass transfer are not the same. Increasing Lewis number causes a partial enhancement in the contribution of irreversibility due to mass transfer in the total entropy generation, while it reduces $\overline{S_T}^{\dagger}$ values. Nevertheless, due to the range of variations, the influence of Lewis number on the contribution of various fluid irreversibilities in the total entropy generation seems to be insignificant.

4.3. Influence of Buoyancy ratio

In fact, the buoyancy ratio has been examined as the ratio of buoyancy forces because of concentration and temperature gradients. The influence of buoyancy ratio on the streamlines and isotherms, when Sr = Df = 0.25 and Ha = 10, is illustrated in Figure 10. Lewis number is set to unity, hereinafter. This implies the existence of similar diffusion characteristics, highlighting the implications of the considered key parameters alone. For negative values of buoyancy ratio, $B < 0$, the thermal and solutal buoyancies act in an opposite way, whereby the primary vortex is divided into two vortices, and also a small anti-clockwise circular vortex is formed at the center of the enclosure. The effective area of the enclosure has a straight relationship with the size of anticlockwise circular vortex, whereby the skewed enclosure with $\lambda = 90°$ has the largest anticlockwise vortex. When $B = 0$, mass transport vanishes and the problem reduces to a pure thermal natural convection. The flow becomes symmetric as the skew angle of skewed enclosure increases. However, the primary vortex moves upwards with further increase of buoyancy ratio. This fact is due to the aiding effect of solutal buoyancy forces in those cases. The solutal buoyancy forces have an aiding or opposing action on thermal buoyancy forces when B is a positive or negative value, respectively. The influence of buoyancy ratio on the isotherm patterns is illustrated in Figure 10(b). A similar case was observed for isoconcentrations, not presented here for the sake of brevity. It can be seen that the isotherms are parallel to the heated bottom wall when B has a negative value. Moreover, the thickness of thermal boundary layer along the bottom wall increased with the increase of buoyancy ratio in all skewed enclosures. The aiding effect of solutal buoyancy against thermal buoyancy forces significantly improves the convective heat transfer across the enclosure.

The influences of buoyancy ratio on the fluid intensity and total kinetic energy are presented in Figure 11(a) and (b), respectively. It can be seen that both of them are enhanced with further increase

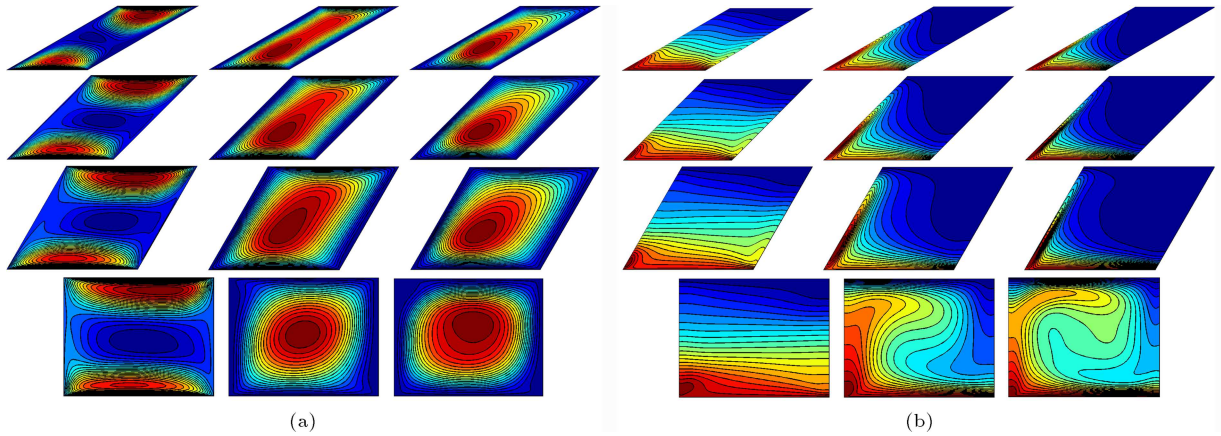

Figure 10. Effect of buoyancy ratio on (a) streamlines and (b) isotherms in four skewed enclosures with $\lambda = 30°, 45°, 60°$, and $90°$, while $B = -10, 0$, and 10 in the first, second, and third columns, respectively, and Ri = 10, Le = 1, Ha = 10, and Df = Sr = 0.25 in all the cases.

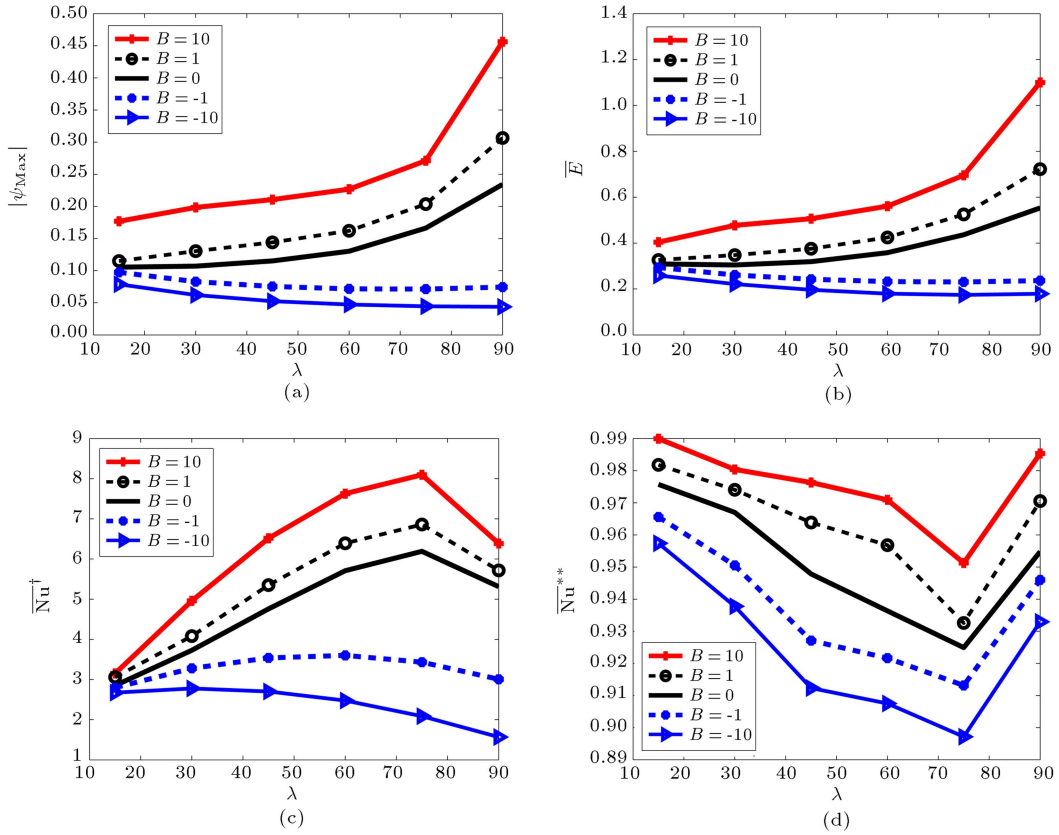

Figure 11. The variations of (a) the absolute value of stream function at primary vortex, (b) the total kinetic energy, (c) the average Nusselt number, and (d) $\overline{Nu}^{**}$ value as a function of skew angle for various buoyancy ratios, while Ri = 10, Le = 1, Ha = 10, and Df = Sr = 0.25.

of buoyancy ratio. Moreover, the aiding action of solutal buoyancy effect on the thermal buoyancy forces is pronounced in skewed enclosures with larger effective areas, whereby the case with $B = 10$ and $\lambda = 90°$ has the largest $|\psi_{Max}|$ value. The effect of buoyancy ratio on the average Nusselt number is characterized in Figure 11(c). It can be seen that $\overline{Nu}$ is reduced with increasing skew angle when B has negative value. This fact is due to the formation of anti-clockwise circular vortex in the cases with $B < 0$, which was strengthened with the increase of the effective area. On the other hand, the average Nusselt number increased with increasing buoyancy ratio. The aiding effect of thermal and solutal buoyancies is again recognized as the main reason of the heat transfer enhancement. The influence of buoyancy ratio on variations in the

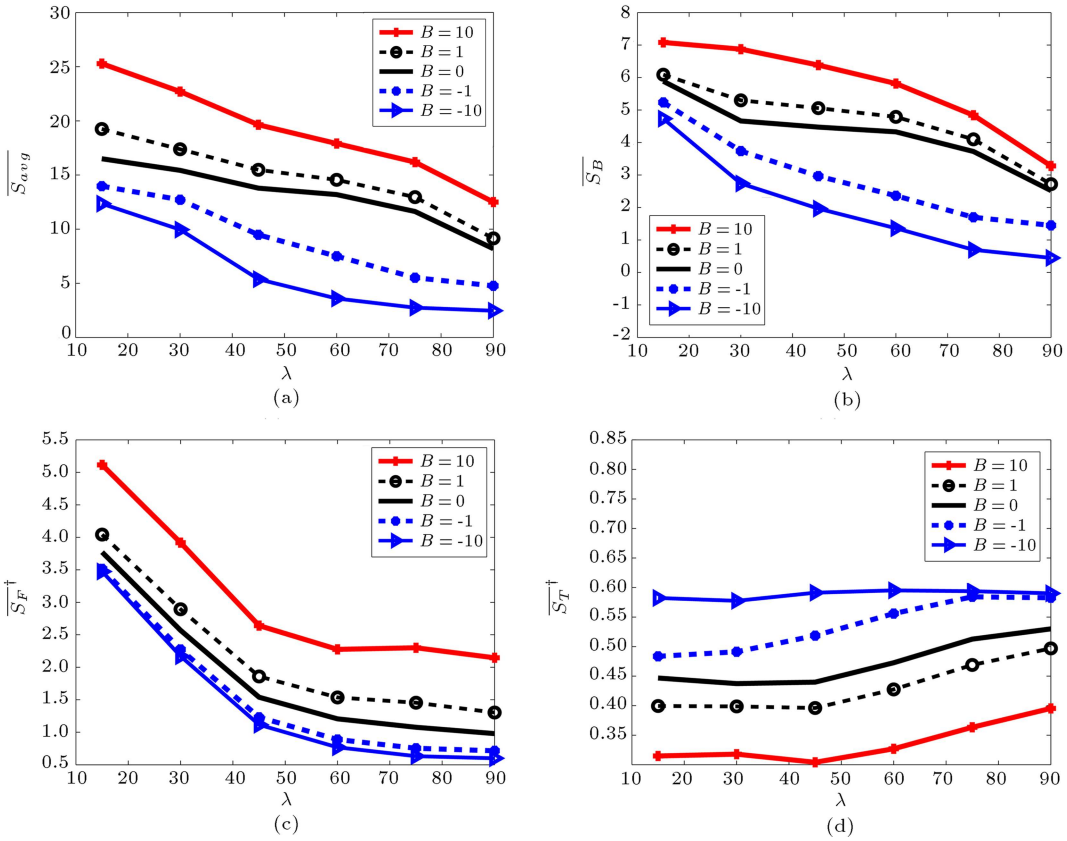

Figure 12. The variations of (a) the average entropy generation, (b) the average entropy generation due to magnetic field irreversibility, (c) the average entropy generation due to fluid friction irreversibility, and (d) $\overline{S_T}^{\dagger}$ value as a function of skew angle for various buoyancy ratios, while Ri = 10, Le = 1, Ha = 10, and Df = Sr = 0.25.

rates of the average Nusselt number, due to applying external magnetic field, is exhibited in Figure 11(d). $\overline{\mathrm{Nu}}^{**}$ values are reduced with decreasing buoyancy ratio. It appears that the suppression effect of Lorentz force is augmented when it is accompanied by the opposing action of solutal buoyancy forces against thermal buoyancy forces.

The effect of buoyancy ratio on the average entropy generation is illustrated in Figure 12(a). As can be seen, the average entropy generation enhances as the buoyancy ratio increases. The variations of $\overline{S_F}$ and $\overline{S_B}$ as a function of λ for various Dufour coefficients are presented in Figure 12(b) and (c), respectively. As can be seen, both of them improve as buoyancy ratio increases. The aiding effect of solutal buoyancy forces on the thermal buoyancy forces improves fluid intensity (see Figure 11(a)), resulting in increasing both $\overline{S_F}$ and $\overline{S_B}$ values (see Eqs. (21) and (24)). In contrast, as can be observed in Figure 12(d), increasing buoyancy ratio decreases the contribution of fluid irreversibility due to thermal effects in the average entropy generation, whereby $\overline{S_T}^{\dagger}$ is a decreasing function of B. It was observed before that the isotherm lines become parallel to the heated wall with reducing buoyancy ratio (Figure 10(b)), whereby the enclosure becomes a quasi-conductive domain in the cases with the largest negative B values. In other words, increasing buoyancy ratio reduces conductive mode of heat transfer, thus decreasing fluid irreversibility due to the thermal effect. However, it is again observed that $\overline{S_T}^{\dagger}$ values improve as the effective area of the skewed enclosure increases.

4.4. Effect of Dufour coefficient

As mentioned earlier, the diffusion of heat caused by concentration gradient is named Dufour effect. Figure 13 represents the influence of Dufour coefficient on the streamlines, isotherms, and isoconcentrations for Sr = 0.25, Ha = 10, Le = B = 1, and Ri = 10. Figure 13(a) exhibits that the effect of Dufour coefficient on streamlines of combined thermos-solutal natural convection is insignificant. Figure 13(b) demonstrates that the thickness of the heat lines along the bottom heated wall increased with an enhancement of Dufour coefficient. However, it seems that the influence of Dufour coefficient is more pronounced with increasing skew angle, which is the effective area of the skewed enclosure. Figure 13(c) depicts the influence of Dufour coefficient on the mass distribution. It can be seen that the enclosures were occupied by the oval-and

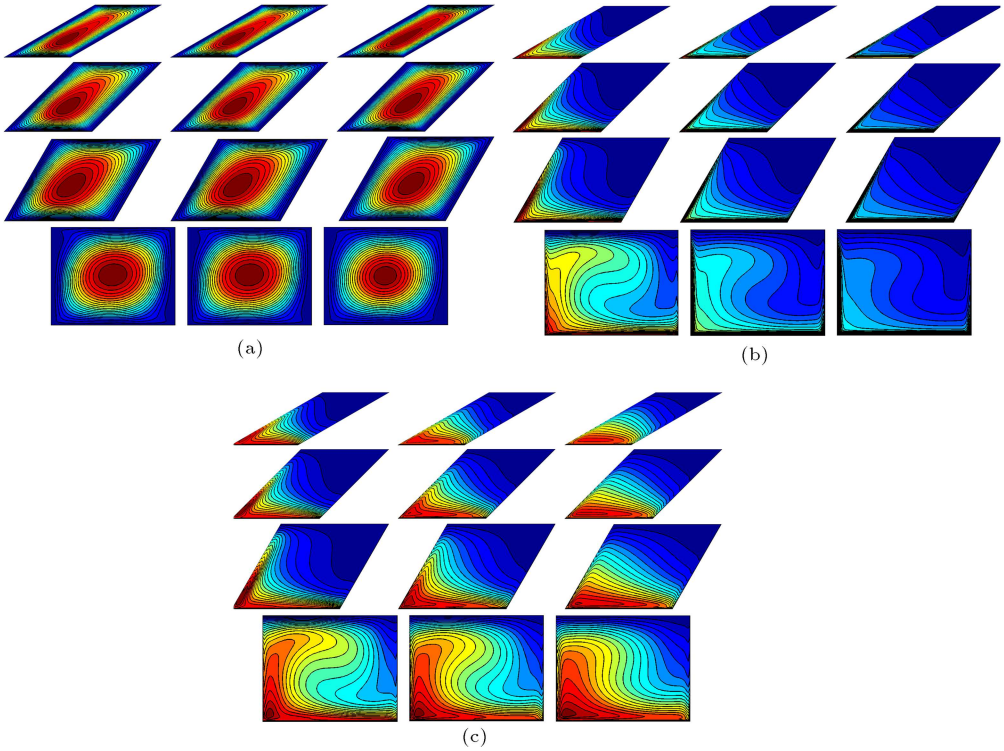

Figure 13. Effects of Dufour coefficient on (a) streamlines, (b) isotherms, and (c) isoconcentrations in four skewed enclosures with $\lambda = 30°, 45°, 60°$, and $90°$, while Df $= 1, 3$, and 7 in the first, second, and third columns, respectively, and Ri $= 10$, Le $= B = 1$, Ha $= 10$, and Sr $= 0.25$ in all the cases.

wavy-shape closed mass lines. Moreover, the wavy-shape mass lines became smooth, while the oval-shape isoconcentrations were attenuated with increasing either skew angle or Dufour coefficient. Those kinds of isoconcentration patterns represent the convective current of mass across the skewed enclosure. Hence, the variations of oval- and wavy-shaped closed mass lines with increasing Dufour coefficient elucidate that the convective mass transfer across the skewed enclosure is improved by increasing the effective area of the skewed enclosure or extra heat due to the concentration gradient.

The effects of Dufour coefficient on the fluid intensity and total kinetic energy are depicted in Figure 14(a) and (b), respectively. It can be seen that the extra heat diffusion caused by the concentration gradient increases both of $|\psi_{\text{Max}}|$ and $\overline{E}$ values. Nevertheless, the influence of Dufour coefficient on $|\psi_{\text{Max}}|$ and $\overline{E}$ values in skewed enclosures with $\lambda < 75°$ appears to be insignificant. The variations of $\overline{\text{Nu}}$ and $\overline{\text{Nu}}^{**}$ as a function of skew angle and for various Dufour coefficients are illustrated in Figure 14(c) and (d), respectively. As can be observed, the heat transfer across the skewed enclosures improves as the extra heat diffusion caused by concentration gradient enhances. Meanwhile, this enhancement is almost uniformly for skewed enclosures with $\lambda \geq 45°$. Figure 14(d) shows that the variation of $\overline{\text{Nu}}^{**}$ depends mainly on λ value. For the cases with $\lambda < 90°$, the reduction rate of heat transfer, due to applying external magnetic field, is accelerated with further enhancement of Dufour coefficient, while the opposite is observed for the cases with $\lambda = 90°$. The variations of $\overline{\text{Sh}}$ and $\overline{\text{Sh}}^{**}$ as a function of skew angle and for various Dufour coefficients are shown in Figure 14(e) and (f), respectively. Figure 14(e) presents that the mass transfer within the skewed enclosures with $\lambda > 30°$ enhances as the Dufour coefficient increases, while the influence of Dufour coefficient on $\overline{\text{Sh}}$ when $\lambda \leq 30°$ seems to be insignificant. In other words, the influence of Dufour coefficient on mass transfer is pronounced with increasing effective area of the skewed enclosure. Figure 14(f) shows that the mass transfer reduction rate, due to applying external magnetic field, $\overline{\text{Sh}}^{**}$, is reduced with decreasing extra thermal diffusion caused by concentration gradient. The influence of Dufour coefficient on the suppression effect of Lorentz force is also pronounced in skewed enclosures with larger skew angles.

The variation of the average entropy generation as a function of λ and for various Dufour coefficients is presented in Figure 15(a). It can be seen that Dufour effect increases the entropy generation in all skewed enclosures. The average entropy generation is also a reducing function of skew angle similar to the previous sections. The variations of entropy

generation due to magnetic field and fluid friction, $\overline{S_B}$ and $\overline{S_F}$, are depicted in Figure 15(c) and (d), respectively. Both of them are reduced with further enhancement of skew angle, as explained before in the previous sections. However, $\overline{S_B}$ is also reduced with reducing Dufour coefficient. This may be due to the direct relationship between fluid intensity and Dufour coefficient which was observed before in Figure 14(a). Besides, Figure 15(c) shows that the influence of Dufour coefficient on $\overline{S_F}$ values seems to be insignificant. The variation of $\overline{S_T}^{\dagger}$ as a function of skew angle for various Dufour coefficients is presented in Figure 15(d). This figure shows that the contribution of the entropy generation due to the thermal effect in the total entropy generation, $\overline{S_T}^{\dagger}$, is increased with increasing Dufour coefficient. Increasing Dufour coefficient improves the conductive mode of heat transfer within the enclosure (see Figure 13(b)), thus increasing fluid irreversibility due to the thermal effects. Meanwhile, the contribution of fluid irreversibility due to thermal effect decreases as the effective area of the skewed enclosure enhances, as shown in the previous sections.

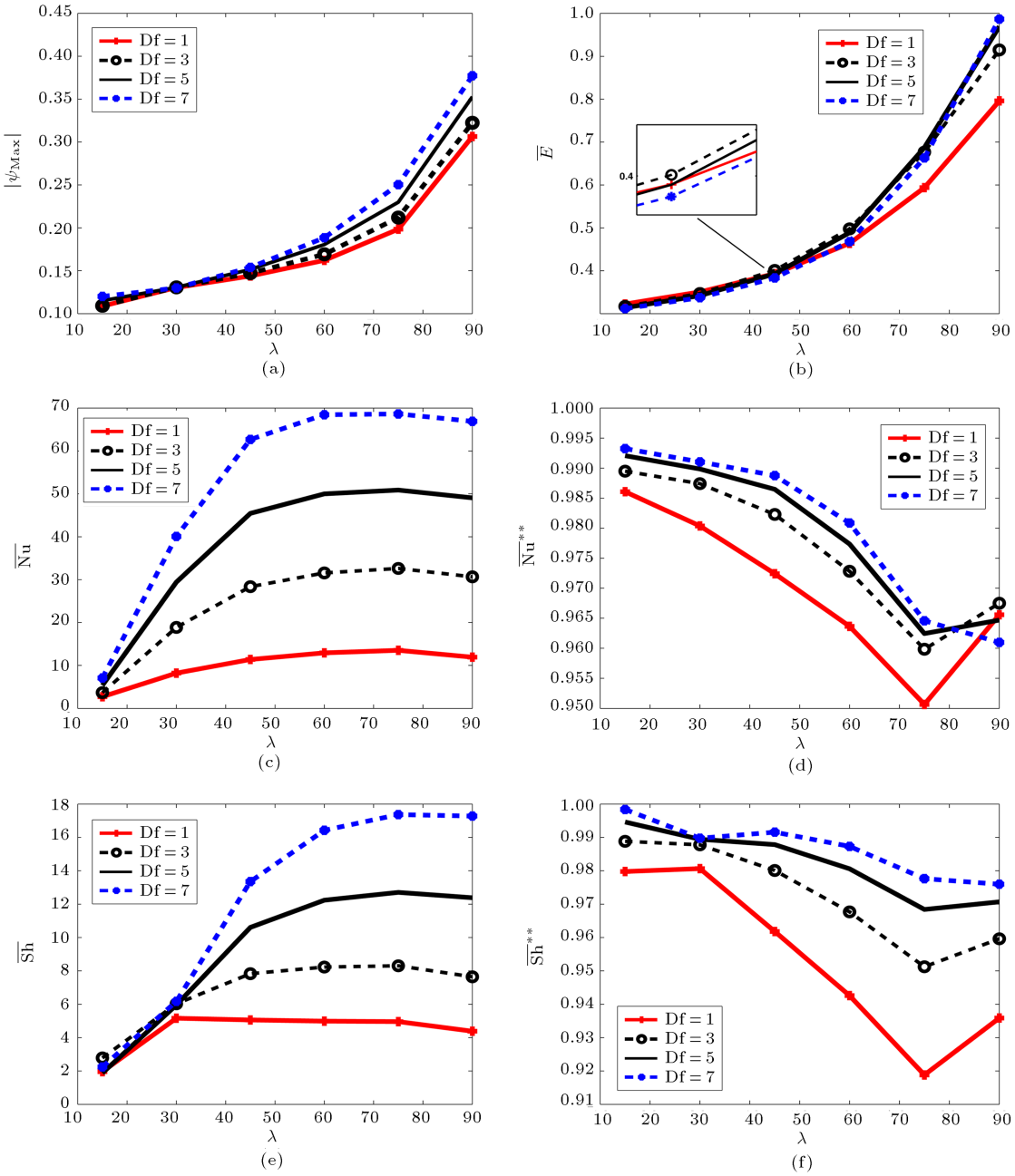

Figure 14. The variations of (a) absolute value of stream function at primary vortex, (b) total kinetic energy, (c) average Nusselt number, (d) $\overline{Nu}^{**}$ value, (e) average Sherwood number, and (f) $\overline{Sh}^{**}$ value as a function of skew angle for various Dufour coefficients, while Ri = 10, Le = B = 1, Ha = 10, and Sr = 0.25.

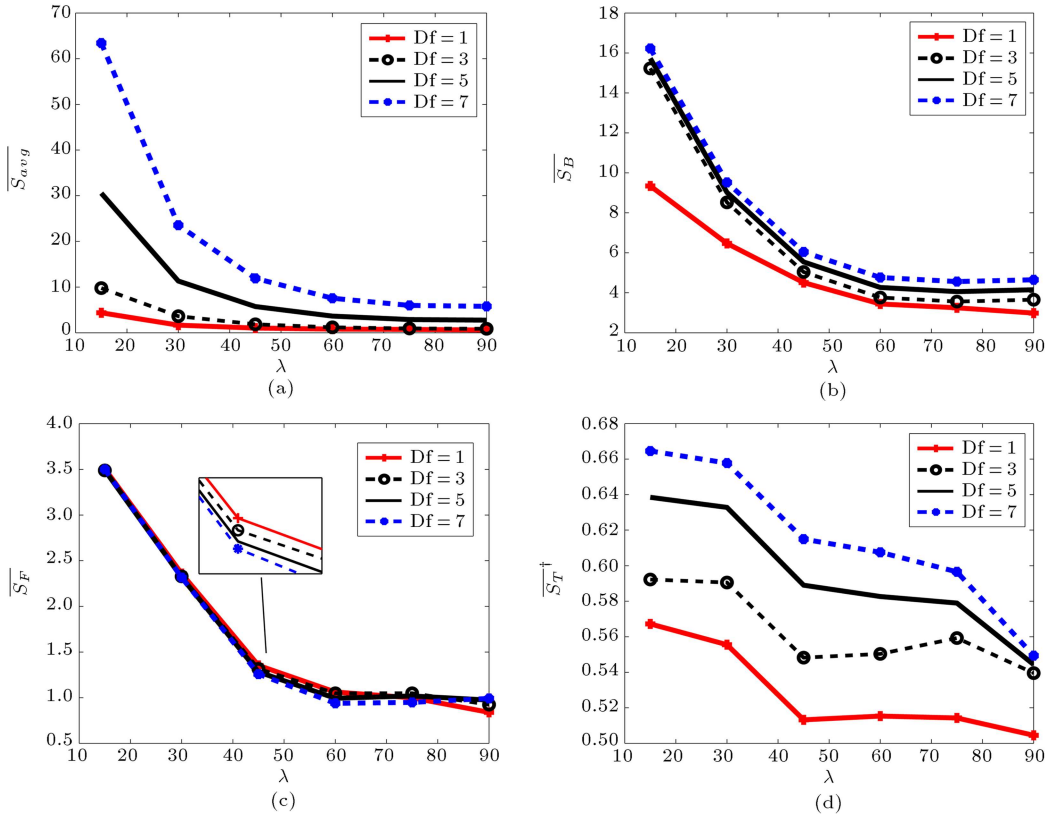

Figure 15. The variations of (a) average entropy generation, (b) average entropy generation due to magnetic field irreversibility, (c) average entropy generation due to fluid friction irreversibility, and (d) $\overline{S_T}^{\dagger}$ value as a function of skew angle for various Dufour coefficients, while Ri = 10, Le = B = 1, Ha = 10, and Sr = 0.25.

5. Summary and conclusion

In this study, fluid flow, heat and mass transfer of combined thermo-solutal natural convection subjected to an external magnetic field and with extra heat and mass diffusions inside a two-sided lid-driven skewed enclosure have been studied numerically. In addition, the entropy generation analysis was conducted to study the affective parameters on the various fluid irreversibilities. A finite volume method based on SIMPLE algorithm is adopted, validated, and utilized to solve the governing equations. The study on the pertinent parameters has been carried out in the following ranges: Hartman number $0 \leq \mathrm{Ha} \leq 30$, Lewis number $1 \leq \mathrm{Le} \leq 50$, buoyancy ratio $-10 \leq B \leq 10$, and Dufour coefficient $0 \leq \mathrm{Df} \leq 7$. Reynolds, Grashof, and Richardson numbers are kept constant at 100, 10, and 10, respectively, while two certain values are assumed for Soret coefficient, i.e. 0 and 0.25. Air is assumed as the working fluid, so the Prandtl number is fixed at 0.71. The simulations are performed in the skewed enclosures with $\lambda = 15°, 30°, 45°, 60°, 75°$, and $90°$. The main findings of this study can be highlighted as follows:

1. The fluid characteristics, heat and mass transfer, as well as the entropy generation are sensitive greatly to the skew angle, effective area, of skewed enclosure. The skewed enclosures with larger skew angles have larger total kinetic energies and fluid intensities, whereas the average entropy generation is minimum at skew angle $\lambda = 90°$;
2. The influence of Lewis number on the fluid intensity and total kinetic energy seems to be insignificant;
3. The mass transfer across the skewed enclosure enhances with rising Lewis number, while the influence of Lewis number on the heat transfer manifests that various fashions mainly depend on the presence of extra heat and mass diffusions, SD-effects;
4. The fluid characteristics, the transport phenomena, as well as the entropy generation are affected to some extent by buoyancy ratio variation. In positive values of buoyancy ratio, the aiding effect of solutal buoyancy forces on the thermal buoyancy forces improves both of heat and mass transfer across the skewed enclosure;
5. The suppression effect of Lorentz force against convective heat transfer is improved by increasing Lewis number, while the external magnetic field causes an enhancement in the mass transfer in the cases with large Lewis numbers. However, the influence of Lorentz force on the mass transfer is attenuated by raising the Lewis number value;

6. The suppression effect of Lorentz force against convective heat and mass transfer is pronounced as buoyancy ratio reduces;
7. The extra heat diffusion caused by concentration gradient, Dufour effect, has an aiding effect on the fluid characteristics, the heat and mass transfer, as well as the entropy generation within the skewed enclosure.

Nomenclature

B	Buoyancy ration
B_0	Magnetic fluid intensity (Wbm^2)
C	Particles concentration (kgm^3)
C_0	Characteristic particles concentration
D_m	Diffusion coefficient ($\mathrm{m}^2\mathrm{s}^{-1}$)
Df	Dimensionless Dufour coefficient
g	Acceleration due to gravity (ms^{-2})
Gr_C	Solutal Grashof number
Gr_T	Thermal Grashof number
Ha	Hartmann number
L	Driven cavity width
Le	Lewis number
Nu	Nusselt number
P	Non-dimensional fluid pressure
p	Fluid pressure (Nm^{-2})
p_0	Pressure scale
Pr	Prandtl number
Re	Reynolds number
Ri	Richardson number
S	Entropy (JK^{-1})
Sc	Schmidt number
Sh	Sherwood number
Sr	Dimensionless Soret coefficient
T	Fluid temperature (K)
T_0	Characteristic fluid temperature
U, V	Non-dimensional velocity components
u, v	Velocity components (ms^{-1})
U_0	Absolute lid velocity (ms^{-1})
X, Y	Non-dimensional Cartesian coordinate
x, y	Cartesian coordinate (m)

Greek

α_m	Thermal diffusivity ($\mathrm{m}^2\mathrm{s}$)
β_C	Concentration expansion coefficient (K^{-1})
β_T	Thermal expansion coefficient (K^{-1})
κ_{CT}	Soret coefficient ($\mathrm{m}^{-1}\mathrm{K}^{-1}\mathrm{kgs}^{-1}$)
κ_{TC}	Dufour coefficient ($\mathrm{m}^5\mathrm{Kkgs}^{-1}$)
ν	Kinematic viscosity of fluid ($\mathrm{m}^2\mathrm{s}^{-1}$)
Φ	Dimensionless particle concentration
ψ	Stream function
ρ	Fluid density (kgm^{-3})
ρ_0	Characteristic fluid density
σ	Electrical conductivity (Sm^{-1})
Θ	Dimensionless fluid temperature

Superscript

B	Magnetic field irreversibility
C	Mass transfer irreversibility
F	Fluid friction irreversibility
h	High temperature and concentration
l	Low temperature and concentration
T	Heat transfer irreversibility

References

1. Oztop, H.F., Zhao, Z., and Yu, B. "Conduction-combined forced and natural convection in lid-driven enclosures divided by a vertical solid partition", *Int. Comun. Heat Mass Transfer*, **36**, pp. 661-668 (2009).
2. Yapachi, K. and Obut, S. "Laminar mixed-convection heat transfer in a lid-driven cavity with modified heated wall", *Heat Transfer Eng.,* **36**, pp. 303-314 (2015).
3. Huppert, H.E. and Sparks, R.S.J. "Double-diffusive convection due to crystalization in magmas", *Ann. Rev. Earth Planet Sci.*, **12**, pp. 11-37 (1984).
4. Nield, D.A. and Kuznetsov, A.V. "The onset of double-diffusive convection in a nanofluid layer", *Int. J. Heat and Fluid Flow,* **32**, pp. 771-776 (2011).
5. Rashidi, M.M. Laraqi, N., and Sadri, S.M. "A novel analytical solution of mixed convection about an inclined flat plate embedded in a porous medium using the DTM-pade", *Int. J. Therm. Sci.,* **49**, pp. 2405-2412 (2010).
6. Nithyadevi, N. and Yang, R-J. "Double-diffusive natural convection in a partially heated enclosure with Soret and Dufour effects", *Int. J. Heat and Fluid Flow,* **30**, pp. 902-910 (2009).
7. Bera, P., Pippal, S., and Sharma, A.K. "A thermal non-equilibrium approach on double-diffusive natural convection in a square porous medium cavity", *Int. J. Heat Mass Transfer*, **78**, pp. 1080-1094 (2014).
8. Wang, J., Yang, M., and Zhang, Y. "Onset of double-diffusive convection in horizontal cavity with Soret and Dufour effects", *Int. J. Heat Mass Transfer*, **78**, pp. 1023-1031 (2014).
9. Al-Amiri, A., Khanafer, K., Bull, J., and Pop, I. "Numerical simulation of combined thermal and mass transport in a square lid-driven cavity", *Int. J. Therm. Sci.*, **46**, pp. 662-671 (2007).

10. Mahapatra, T.R., Pal, D., and Mondal, S. "Effects of buoyancy ratio on double-diffusive natural convection in a lid-driven cavity", *Int. J. Heat Mass Transfer*, **57**, pp. 771-785 (2013).

11. Azad, A.K., Munshi, M.J.H., and Rahman, M.M. "Double-diffusive mixed convection in a channel with a circular heater", *Procedia Engineering*, **56**, pp. 157-162 (2013).

12. Kareem, A.K., Gao, Sh., and Ahmed, A.Q. "Unsteady simulations of mixed convection heat transfer in a 3D closed lid-driven cavity", *Int. J. Heat Mass Transfer*, **100**, pp. 121-130 (2016).

13. Bettaibi, S., Kuznik, F., and Sediki, E. "Hybrid LBM-MRT model coupled with finite difference method for double-diffusive mixed convection in rectangular enclosure with insulated moving lid", *Physica A: Statistical Mechanics and Its Applications*, **444**, pp. 311-326 (2016).

14. Wang, L., Shi, B., Chai, Z., and Yang, X. "Regularized lattice Boltzmann model for double-diffusive convection in vertical enclosures with heating and salting from below", *Appl. Thermal Eng.*, **103**, pp. 365-376 (2016).

15. Kefayati, Gh.R. "Mesoscopic simulation of magnetic field effect on double-diffusive mixed convection of shearthinning fluids in a two sided lid-driven cavity", *J. Molec. Liquids*, **198**, pp. 413-429 (2014).

16. Mondal, S. and Sibanda, P. "Unsteady double diffusive convection in an inclined rectangular lid-driven enclosure with different magnetic field angles and non-uniform boundary conditions", *Int. J. Heat Mass Transfer*, **90**, pp. 900-910 (2015).

17. Borhan Uddin, M., Rahman, M.M., Khan, M.A.H., and Ibrahim, T.A. "Effect of buoyancy ratio on unsteady thermosolutal combined convection in a lid driven trapezoidal enclosure in the presence of magnetic field", *Comput. Fluids*, **114**, pp. 284-296 (2015).

18. Rebi, L.K., Mojtabi, A., Safi, M.J., and Mohammad, A.A. "Numerical study of thermo-solutal convection with Soret effect in a square cavity", *Int. J. Heat Fluid Flow*, **18**, pp. 561-579 (2008).

19. Bhuvaneswari, M., Sivasankaran, S., and Kim, Y.J. "Numerical study on double-diffusive mixed convection with a Soret effect in a two-sided lid-driven cavity", *Num. Heat Transfer A*, **59**, pp. 543-560 (2011).

20. Kefayati, Gh.R. "FDLBM simulation of entropy generation in double diffusive natural convection of power-law fluids in an enclosure with Soret and Dufour effects", *Int. J. Heat and Mass Transfer*, **89**, pp. 267-290 (2015).

21. Kefayati, Gh.R. "Simulation of double diffusive natural convection and entropy generation of power-law fluids in an inclined porous cavity with Soret and Dufour effects (Part I: Study of fluid flow, heat and mass transfer)", *Int. J. Heat and Mass Transfer*, **94**, pp. 539-581 (2016).

22. Ren, Q. and Chan, C.L. "Numerical study of double-diffusive convection in a vertical cavity with Soret and Dufour effects by lattice Boltzmann method on GPU", *Int. J. Heat and Mass Transfer*, **93**, pp. 538-553 (2016).

23. Qu, Z.G., Tao, W.Q., and Hw, Y.L. "An improved numerical scheme for the SIMPLER method on nonorthogonal curvilinear coordinates: SIMPLERM", *Num. Heat Transfer Part B: Fundam.*, **51**, pp. 43-66 (2007).

24. Al-Farhany, K. and Turan, A. "Numerical study of double diffusive natural convective heat and mass transfer in an inclined rectangular cavity filled with porous medium", *Int. Commun. Heat Mass Transfer*, **39**, pp. 174-181 (2012).

25. Chamkha, A.J., Hussain, S.H., and Ali, F.H. "Conduction-combined forced and natural convection in a lid-driven parallelogram-shaped enclosure divided by a solid partition", *Progress in Comput. Fluid Dyn.*, **12**, pp. 309-321 (2012).

26. Jagadeesha, R.D., Prasanna, B.M.R., and Sarkar, M. "Double diffusive convection in an inclined parallelogrammic porous enclosure", *Procedia Engineering*, **127**, pp. 1346-1353 (2015).

27. Nayak, R.K., Bhattacharyya, S., and Pop, I. "Numerical study on mixed convection and entropy generation of Cu-water nanofluid in a differentially heated skewed enclosure", *Int. J. Heat Mass Transfer*, **85**, pp. 620-634 (2015).

28. Goyan, O. "High-Reynolds number solutions of Navier-Stokes equations using incremental unknowns", *Comput. Method. Appl. Mech. Eng.*, **130**, pp. 319-335 (1996).

29. Chen, Sh., Xiao, X., and Zheng, Ch. "Analysis of entropy generation in double-diffusive natural convection of nanofluid", *Int. J. Heat Mass Transfer*, **87**, pp. 447-463 (2015).

30. Kefayati, Gh.R. "Simulation of double diffusive natural convection and entropy generation of power-law fluids in an inclined porous cavity with Soret and Dufour effects (Part II: Entropy generation)", *Int. J. Heat and Mass Transfer*, **94**, pp. 582-624 (2016).

31. Patankar, S.V., *Numerical Heat Transfer and Fluid Flow*, Hemisphere, Washington D.C. (1980).

32. Screiber, R. and Keller, H.B. "Driven cavity flows by efficient numerical techniques", *J. Comput. Phys.*, **49**, pp. 310-333 (1983).

33. Kuhlmann, C., Wanschura, M., and Rath, H.J. "Flow in two-sided lid-driven cavities: Non-uniqueness, instabilities, and cellular structures", *J. Fluid Mech.*, **336**, pp. 267-299 (1997).

34. Demirdzic, I., Lilek, Z., and Peric, M. "Fluid flow and heat transfer test problems for non-orthogonal grids: Bench-mark solutions", *Int. J. Num. Meth. Fluids*, **15**, pp. 329-354 (1992).

35. Ghaffarpasand, O. "Numerical study of MHD natural convection inside a sinusoidally heated lid-driven cav-

ity filled with Fe3O4-water nanofluid in the presence of Joule heating", *Appl. Math. Mod.*, **40**, pp. 9165-9182 (2016).

36. Erturk, E. and Dursun, B. "Numerical solutions of 2-D steady incompressible flow in a driven skewed cavity", *J. Appl. Math. Mech. (ZAMM)*, **87**, pp. 71-78 (2007).
37. Hussein, S.H. and Hussain, A.K. "Natural convection heat transfer enhancement in a differentially heated parallegramic enclosure filled with copper-water nanofluid", *ASME J. Heat Transfer,* **136**, pp. 82502-82508 (2014).
38. Teamah, M.A. and El-Maghlany, W.M. "Numerical simulation of double-diffusive mixed convection in rectangular enclosure with insulated moving lid", *Int. J. Therm. Sci.,* **49**, pp. 1625-1638 (2010).

Biography

Omid Ghaffarpasand received his PhD from the Department of Physics, University of Isfahan, Iran in 2012. Currently, he is a full-time faculty member at the Department of Physics, University of Isfahan, Iran. His current research fields include fluid dynamics, computational fluid dynamics, Aerosol technology, Aerosol propagation and deposition mechanisms, heat transfer and fluid flow of magnetohydrodynamic convection.